A. Tricoli, A. Teleki, and M. Righettoni

DOI: 10.1002/anie.200903801

Semiconductor Sensors

Semiconductor Gas Sensors: Dry Synthesis and Application

Antonio Tricoli, Marco Righettoni, and Alexandra Teleki**

Keywords:
aerosols · nanomaterials · semiconductors · sensors

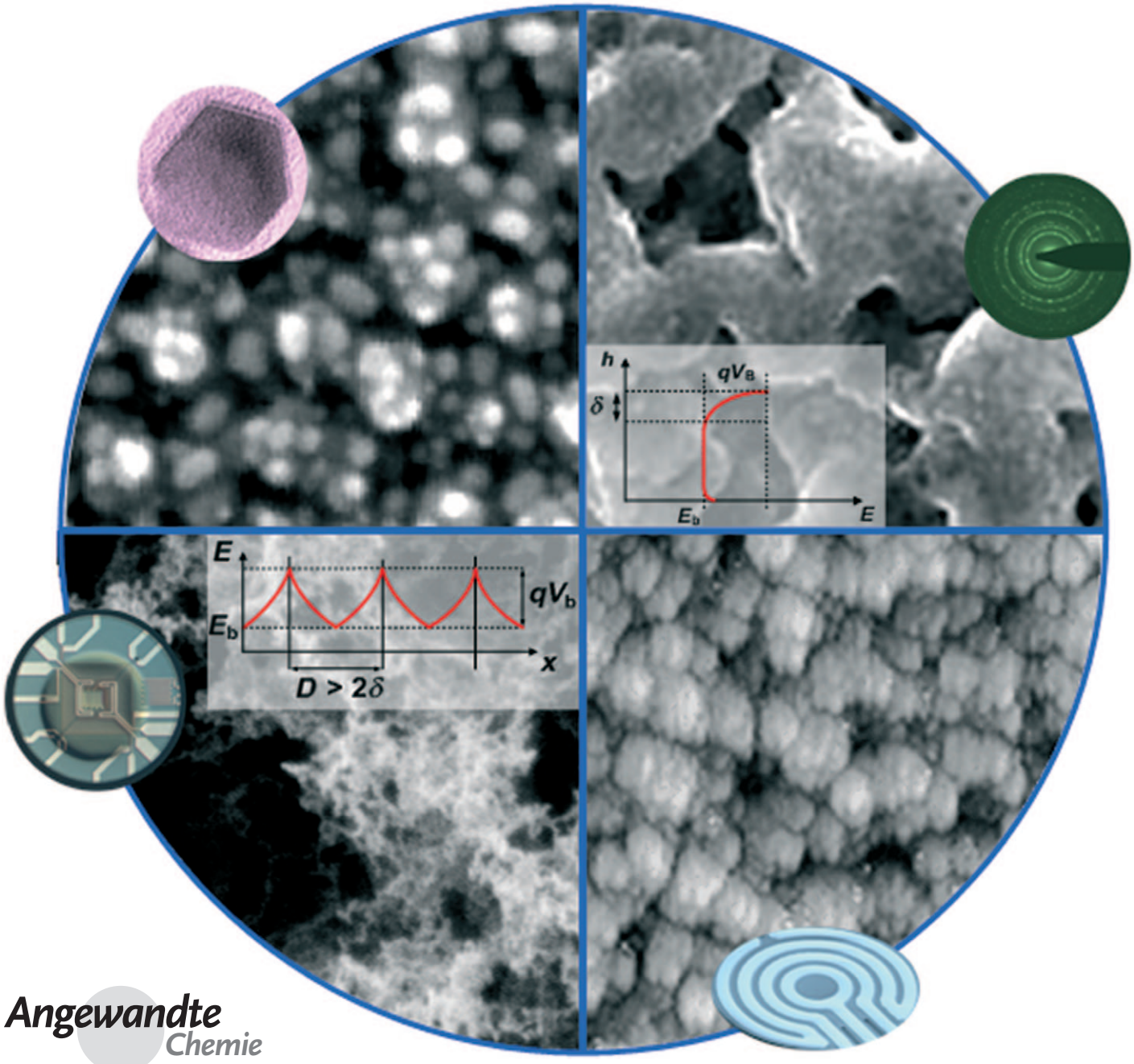

Since the development of the first chemoresistive metal oxide based gas sensors, transducers with innovative properties have been prepared by a variety of wet- and dry-deposition methods. Among these, direct assembly of nanostructured films from the gas phase promises simple fabrication and control and with the appropriate synthesis and deposition methods nm to μm thick films, can be prepared. Dense structures are achieved by tuning chemical or vapor deposition methods whereas particulate films are obtained by deposition of airborne, mono- or polydisperse, aggregated or agglomerated nanoparticles. Innovative materials in non-equilibrium or sub-stoichiometric states are captured by rapid cooling during their synthesis. This Review presents some of the most common chemical and vapor-deposition methods for the synthesis of semiconductor metal oxide based detectors for chemical gas sensors. In addition, the synthesis of highly porous films by novel aerosol methods is discussed. A direct comparison of structural and chemical properties with sensing performance is given.

From the Contents

1. Introduction

The sensorial perception of the surroundings is critically related to the development of animal and human life. Sharp sight, touch, taste, hearing, and smell have determined the evolution of species and their endurance throughout the centuries. Human smell, or more generally, gas detection is a complex sensorial experience that subtly influences our decisions and actions. In general, it can be correlated to attraction or repulsion toward specific gas mixtures and their sources, which has implication in nutrition, safety, reproduction, and healthcare. The capability to differentiate between sour and ripe vegetables, fresh and rotten meats, drinkable water, to name a few examples, is fundamental to avoid toxins and assure a correct nutrition. Nevertheless, the human olfactory system is limited to a qualitative detection of a few gases. In fact, while the smell of fire successfully alerts and thereby saves lives, the inability of humans to detect poisonous CO, suffocating CO_2, and explosive CH_4 or H_2 gases has fatal consequences.[1,2] As a result, olfactory aids, such as canaries and safety lamps, have been utilized in dangerous environments (e.g. coal mines).

The industrial development in the last decades together with the drastic improvement of life quality and mobility has increased the needs for quantitative detection of different analytes.[3] Online analysis of gas mixtures is fundamental to quality control in industrial production,[4] in environmental protection, and assuring safety in the work place. Detection of explosive gases has become consequently more important with the enlargement of centralized methane distribution networks[5] and increasing H_2 production for its possible utilization as fuel.[6] Air-quality monitoring in urban areas and corresponding traffic restriction has become mandatory, as a result of the massive employment of cars producing harmful CO, NO_x, SO_2, soot particles, and hydrocarbons.[7] Modern alcohol breath analyzers based on ethanol sensors are replacing traditional methods for the identification of drunken drivers.[8] Furthermore, recent success in non-invasive medical diagnostics based on human breath analysis is pushing the development of extremely sensitive gas sensors cable of sub-ppm detection of specific analytes (e.g. acetone) in a complex gas mixture.[1,9]

Metal oxide based gas sensors have been developed in the second half of the 20th century and are applied either as chemoresistive (semiconductor) or catalytic/thermal conductivity (hot wire) sensors.[2] The latter evolved from the bare platinum coils utilized for the detection of combustible gases in mines. The heat generated by gas combustion on the platinum-coil surface produced a change in its resistance which was detected by a simple Wheatstone bridge circuit. These first bare platinum-coil sensors suffered from strong drift and short life-time because of their high operation temperature (800–1000 °C), required to oxidize the target gas (e.g. methane). To reduce the operation temperature (e.g. to 500 °C), the catalytic material was later spread on ceramic pellets surrounding the platinum wire/coil. The lower operation temperature vastly reduced the evaporation of the platinum coil improving the sensor long-term stability and its power consumption. This key innovation enabled the fabrication of battery-powered, portable gas sensors which have been commercialized mainly as Pellistor (from "pellet" and "resistor").[2]

[*] Dr. A. Tricoli, M. Righettoni, Dr. A. Teleki
Department of Mechanical and Process Engineering, ETH Zürich
Sonneggstrasse 3, 8092 Zürich (Switzerland)
Fax: (+41) 44-632-1276
E-mail: tricoli@ptl.mavt.ethz.ch
teleki@ptl.mavt.ethz.ch
Homepage: http://www.ptl.ethz.ch

In contrast to Pellistor, chemoresistive gas sensors are based on the electrical properties of semiconductor metal oxides. Following the discovery that the adsorption and desorption of gases causes a change in the electrical conductivity of semiconductors and that at high temperatures (e.g. 400 °C) this process takes place rapidly, a first attempt was made to use ZnO thin films as chromatographic detectors (Figure 1 a) instead of the standard thermal conductivity cell.[10] The preliminary results were promising with the novel (semiconductor) detector having longer response and recovery times, as a result of the adsorption and desorption of the analyte, but about 100-times higher sensitivity than the thermal conductivity cells.[10] This new kind of detector attracted the interest of the gas-chromatography community[15] and shortly after the sensing properties of several metal oxides were investigated, with ZnO, CdO, Fe_2O_3, and SnO_2 being the most sensitive.[16]

Despite their high sensitivity, ZnO thin films had poor long-term stability limiting their immediate application in gas chromatography.[16] Therefore, it was proposed to replace the fragile and expensive thin film by a more robust thick film made of sintered or compressed metal oxide powders equipped with an internal heater (Figure 1 b).[11] This small and low-cost device found its way to the market and SnO_2-based sensors were applied successfully to detection of explosive-gas leakage.[17] Similar SnO_2 devices are still commercialized as Figaro sensors (Figaro Engineering Inc.).

Since these first achievements (Figure 1 a,b) different types of sensor substrates have been investigated including cylindrical (Figure 1 c) and planar (Figure 1 d) sensing-film layouts.[12] The latter are the most promising for integration in micro-machined devices.[18] Solid-state semiconductor gas sensors have a high miniaturization potential as they do not require optical components (as, for example, in IR spectroscopy) or movable parts (e.g. cantilevers). Integration of SnO_2-based films in complementary metal oxide semiconductor (CMOS) gas sensor microsystems[19] based on micro-hotplate technology[13] (Figure 1 e) has enabled the fabrication of fully integrated chips with dimensions on the order of a few mm^2 and even portable micro gas-sensor arrays.[20] Furthermore, optimization of the micro-hotplate layout could increase both detector density and control over the sensor operational parameters (e.g. temperature ramps).[14]

The development of these multifunctional, miniature sensor devices (Figure 1) has been accompanied by efforts to better understand[21–27] their key constituent: the semiconductor metal oxide. The sensing properties of these materials, especially those of SnO_2, have been improved by decreasing their size to the nanoscale and by the addition of appropriate dopants.[3,26,28] Thus, the lower limit of detection and sensitivity were improved by the use of nanostructured materials with grain sizes comparable to twice their Debye length.[29–32] Finely dispersing catalyst nanoparticles, such as Pt,[33–35] Pd,[33,36,37] Ag,[38,39] Ru,[40] and Au[41,42] on the metal oxide surface, further increased the sensitivity, mainly by spill-over effects. Nevertheless, the long-term stability at the operating temperature (typically 250–600 °C) of these highly sensitive materials composed of oxide[30,32,43] and dopant[41,44] components is still challenging. This control is complicated by the often opposing trends of sensitivity and stability: an improvement in sensor stability is accompanied by a loss in sensitivity (e.g. by grain growth during heat treatment).[26]

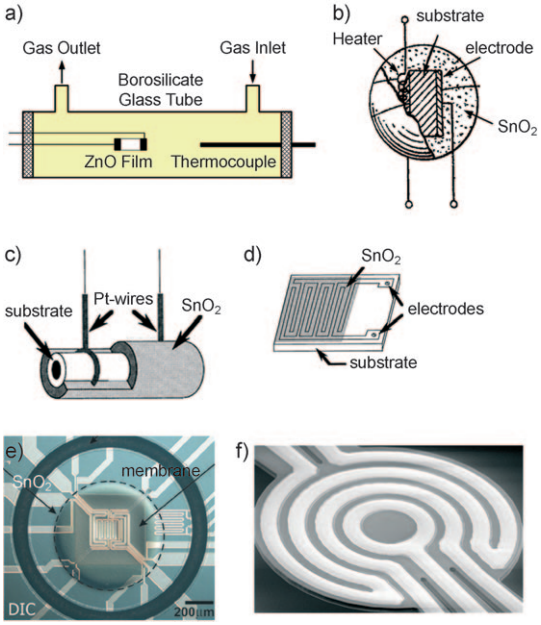

Figure 1. a) Metal oxide thin film utilized as chemoresistive detector for gas chromatography.[10] The adsorption and desorption of the analyte on the hot (ca. 400 °C) metal oxide surface rapidly changes the film resistance allowing its quantitative detection. Representative layouts for portable semiconductor metal oxide gas sensors: b) first thick-film gas-sensor prototype with internal heater;[11] c) sintered-block gas sensor;[12] d) planar-film gas sensor with interdigitated electrodes;[12] e) modern micro-hotplate gas sensor;[13] f) suspended micro-hotplate with circular platinum heaters.[14]

Antonio Tricoli was born in 1981 in Crotone, Italy. He received his Master of Science in Mechanical and Process Engineering from the ETH Zurich in 2004. He joined the Particle Technology Laboratory at ETH Zurich and received his Ph.D. in 2009. He is currently Lecturer and Research Associate at ETH Zurich. His research interests focus on the gas-phase synthesis of semiconductor and dielectric nanoparticles and their utilization for surface functionalization with application in sensors, actuators, fuel and solar cells.

Marco Righettoni was born in 1984 in Lugano, Switzerland. He received his Master of Science in Mechanical Engineering from the ETH Zurich in 2009. He is currently a Ph.D. student at the Particle Technology Laboratory, ETH Zurich. His research interests are in the deposition of nanoparticulate semiconductor films and their utilization for surface functionalization and also their application in sensors for breath analysis diagnostics.

The synthesis method is one of the most crucial parameters to control the sensing properties of the final metal oxide, especially with respect to sensitivity and long-term stability.[26] Film porosity, crystal orientation, oxide stoichiometry, defects/impurity concentration, sinter neck and grain sizes are strictly governed by the process utilized. A first historical classification distinguishes between wet methods and dry methods producing mainly thick and thin films, respectively. In comparison to classical thin films deposited by chemical vapor deposition (CVD) or sputtering, the main advantage of wet methods is the separate processing of the metal oxide and film. This separation allows the production of tailored and stabilized nanoparticles prior to their assembly in films (e.g. by screen printing, drop-, dip-, and spin-coating, doctor blading) resulting in high sensitivity and reasonable stability.[30] However, reproducibility of the sensing films prepared by wet methods is generally poor[45] as a result of crack formation during evaporation of solvents and additives.[46] The thermal and mechanical stress present during film formation can also be a difficulty when applied to sophisticated but fragile micro gas-sensor[18] substrates. Furthermore, control over the film thickness[47] and grain neck[48] sizes is limited, impeding sensor response optimization. Novel dry methods[39,49–51] based on the direct deposition of tailored nanoparticles from an aerosol source, could combine the advantages of wet and classical dry synthesis methods: these are the control over grain[30] and film[26] properties, respectively. These scalable aerosol technologies[52] along with advanced deposition methods, such as electrodynamic focusing,[53] could allow large-scale fabrication of nano-sensor arrays with unprecedented detector densities. One of the main challenges of such novel approaches lies in the stabilization of the mostly physically bounded, porous films as their mechanical stability is generally poor.[51]

Several aspects of ongoing research on semiconducting metal oxides have been reviewed in the last few decades. Most Reviews have focused on material properties, differentiating the various pure and doped metal oxide materials,[3] and analyzing the effect of, for example, crystal size on sensor sensitivity,[21,29,48] structural stability[26] and selectivity.[25,54] Nanomaterials in general have been identified to improve the performance of sensors, especially regarding sensitivity.[55,56] The size as well as the shape of nanomaterials is tunable, for example, in the form of particles, rods, wires, quantum dots, and core–shell structures, which determine their chemical, optical, magnetic, and electronic properties. Their surface chemistry is also tunable and can be exploited for chemo- and biosensors.[57] The application of specific nanostructures as gas sensors has been reviewed, for example, nanowires,[58] carbon nanotubes,[1] and hollow oxides.[59] The sensing mechanism of semiconductor gas sensors has also been addressed both experimentally by in situ and operando spectroscopic techniques to follow the physicochemical processes taking place in an active sensing element in real time and under operating conditions,[60] and theoretically.[21,23–25,27,48]

Several Reviews have shown the importance of structural parameters (pore size, film morphology, surface accessibility) besides the material properties (crystal size, agglomeration, sinter necks).[55,61] The control of these structural parameters is difficult by conventional synthesis methods, such as sol–gel processes, as they are interdependent (e.g. grain size, grain interconnectivity, pore size and pore architecture).[61] Dry synthesis of metal oxides can improve the control over both material properties and film structural parameters. In this Review, an overview of classical[62] dry and novel aerosol methods for synthesis of semiconductor-based sensing films is given. The materials and films obtained by the various processes are discussed and classified in terms of structural parameters and performance, highlighting some fundamental differences with respect to the large spectrum of applicable synthesis methods. Some of these dry methods have been reviewed specifically, for example matrix-assisted pulsed-laser evaporation,[63] pulsed-laser ablation,[58] atomic layer deposition,[64] flame synthesis,[65] pulsed-laser deposition and reactive molecular-beam epitaxy.[66] Herein, the focus is on engineering aspects of synthesis methods that allow functional design of sensing films. For a deeper understanding of the gas-sensing mechanism of semiconductor MO_x, refer to the following Reviews.[24,25,27,60]

Alexandra Teleki received her Master of Science in Chemical Engineering from the Royal Institute of Technology, Stockholm (Sweden) in 2003 and her Ph.D. from the Department of Mechanical and Process Engineering at the ETH Zurich in 2008. She is currently a Lecturer and Research Associate at the Particle Technology Laboratory at ETH. Her research interests are gas-phase material synthesis and nanoparticle surface functionalization for applications in catalysis, gas sensing, and nanocomposites.

2. Detection Mechanism in Semiconductor Gas Sensors: SnO_2

The development of semiconductor films for gas sensors is strictly dependant on their sensing mechanism. Knowledge of their working principles is necessary to evaluate and differentiate between the wide variety of methods capable of producing metal oxide films with nano-sized crystals and grains. A first classification is made between n-type semiconductors (in which electrons are the majority carriers) and p-type (in which the holes are the majority carriers) semiconductors. The conductivity of n-type semiconductors is increased upon contact with a reducing analyte and decreased with an oxidizing one. In contrast, p-type semiconductors (e.g. CuO) have the opposite response. Herein, a brief introduction to the sensing mechanism of n-type metal oxides in dry air is given based on the example of SnO_2 (Figure 2). In fact, among the broad variety of metal oxides tested as gas detectors, SnO_2 has been subject to the largest number of studies.[3,21,23] Its sensing behavior to ethanol[21] and CO[24,25] provides the definitive example for the interplay between adsorbed surface species and conductivity in metal oxide semiconductors. It has set the basis for two general descrip-

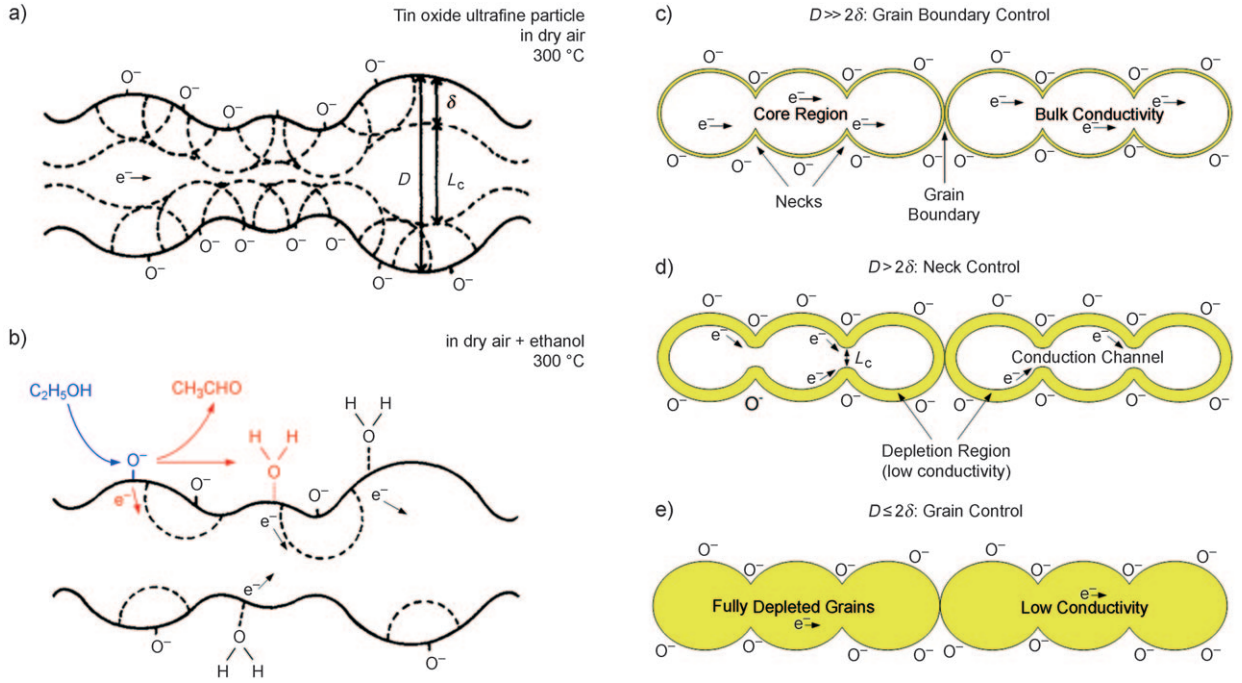

Figure 2. Schematic model of oxygen ionosorption on the SnO_2 surface in a) pure dry air and b) with ethanol.[21] The adsorbed oxygen species (a) trap electrons from SnO_2 forming ions that scatter electrons within the Debye length δ of the oxide (3 nm for SnO_2 at 250 °C).[21] This decreases the electron concentration and mobility resulting in a reduction of the SnO_2 conductivity. The reaction between ethanol and the ionosorbed oxygen (b) decreases the concentration of these scattering centers (O^-) and releases the trapped electrons thereby increasing the SnO_2 conductivity. The mechanism controlling the conductivity change and its magnitude depends mainly on the ratio between grain size (D) and Debye length.[48] If $D \gg \delta$ (c), the depletion of the surface between the grain boundaries controls the conductivity variation. In this case low sensitivity to the analyte is expected as only a small part of the semiconductor is affected by interaction with the analyte. If $D > 2\delta$ (d), a conduction channel with high conductivity exists but its wideness (L_c) is controlled by the surface concentration of oxygen ions leading to moderate sensitivities. If $D \leq 2\delta$ (e), the whole grain is depleted and changes in the surface oxygen concentration affects the whole semiconductor resulting in high sensitivity.[48]

tions[60] of the sensing mechanism: the oxygen-vacancy model (reduction–reoxidation mechanism)[60,67] and the ionosorption[21,24,25,68] model. Neither the ionosorption nor the oxygen-vacancy model can describe all the experimental observations.[60] Herein, we mainly concentrate on the ionosorption model which will serve as a guideline for understanding the structural–functional relations of nanostructured sensing films obtained by several dry synthesis methods.

2.1. The Oxygen-Vacancy Model (Reduction–Reoxidation Mechanism)

This model has been reviewed in detail recently[60] and thus only a short summary is given. The interaction between a gas and a metal oxide is described by the partial reduction and reoxidation of its surface. More specifically, SnO_2 is a n-type semiconductor with oxygen vacancies acting as electron donors. In this framework, the partial reduction of its surface by reaction with a reducing analyte (e.g. CO, EtOH) leads to formation of further oxygen vacancies and thereby injection of free electrons in its conduction band (increased conductivity).[60] Once the reducing analyte is removed, the surface is reoxidized (if oxygen is present) filling the vacancy and reducing the conductivity [Eq. (1)–(3); v_o^x = neutral oxygen vacancy, $v_o^{\bullet}$ = single ionized oxygen vacancy, O_o^x = neutral lattice oxygen, $_{(g)}$ = gas phase].[60]

$$CO_{(g)} + O_o^x \rightleftharpoons CO_{2(g)} + v_o^x \quad (1)$$

$$v_o^x \rightleftharpoons v_o^{\bullet} + e^- \quad (2)$$

$$2\,v_o^{\bullet} + O_{2(g)} + 2\,e^- \rightleftharpoons 2\,O_o^x \quad (3)$$

The opposite mechanism is proposed for oxidizing analytes (e.g. NO_x). The role of vacancy diffusion in the metal oxide bulk is strongly material and temperature dependent and requires further understanding. Furthermore, surface reduction–reoxidation mechanisms at the operating temperatures of SnO_2 gas sensors (ca. 250–450 °C) are relatively slow in comparison to the small response times of such devices[60] suggesting that also other mechanisms (e.g. chemisorptions) could play a significant role.

2.2. Ionosorption Model

2.2.1. Analyte Detection by SnO_2: Reception Function

In the ionosorption model, the detection of gases by SnO_2 films can be subdivided in a reception and a transduction

function.[21,24,25] The adsorbed oxygen species are considered as free oxygen ions electrostatically stabilized on the oxide surface (Figure 2a).[68] Initially, the oxygen is physisorbed on the oxide surface, thereafter electrons are transferred from the metal oxide to the oxygen which is charged and thereby ionosorbed.[21,22,27] Several oxygen species are adsorbed including molecular (O_2^-) and atomic (O^-, O^{2-}) ions. In general, below 150 °C the molecular form dominates while above this temperature the atomic species are found.[24] These adsorbed ions scatter electrons within the Debye length δ of the metal oxide forming a depleted region (Figure 2a) with reduced electron mobility near the oxide surface.[21]

The reception function of SnO_2 (in air) for a reducing or oxidizing analyte, consists in the variation of the ionosorbed oxygen concentration.[21,25] If a reducing analyte is inserted, such as EtOH, H_2 or CO, the surface concentration of oxygen ions is decreased as a result of its partial or complete oxidation (Figure 2b) releasing the trapped electrons and reducing the concentration of scattering centers and thereby increasing the electron mobility in the oxide.[21] The following simplified sensing surface reactions have been suggested for EtOH,[21] H_2,[69] and CO [Eq. (4)–(6)],[48]

$$C_2H_5OH_{(g)} + O_{(ad)}^- \rightleftharpoons CH_3CHO_{(g)} + H_2O_{(g/ad)} + e^- \quad (4)$$

$$H_{2(g)} + O_{(ad)}^- \rightarrow H_2O_{(g)} + e^- \quad (5)$$

$$CO_{(g)} + O_{(ad)}^- \rightarrow CO_{2(g)} + e^- \quad (6)$$

where the analytes are initially in the gas phase (g) and react with the adsorbed (ad) oxygen ions on the SnO_2 surface. In contrast, oxidizing analytes (e.g. NO_x) have an opposite effect by increasing the concentration of ionosorbed oxygen.[70] However, it should be noted that only poor spectroscopic evidence of the oxygen ions' contribution have been collected in situ during gas detection.[27,60]

2.2.2. *Response of SnO_2 to an Analyte: Transduction Function*

After the reception (detection) of an analyte by a change in ionosorbed oxygen concentration, the conductivity of SnO_2 is quantitatively varied in compliance with its transduction function. In fact, although the injection of free charges into the metal oxide is directly proportional to the available ionosorbed oxygen sites for reaction with the analyte, the actual change in electron mobility, which is a result of the change in scattering-center concentration (Figure 2b), depends drastically on the SnO_2 grain morphology.[21,48]

In more detail, the ionosorbed oxygen scatters electrons within the Debye length of SnO_2 reducing its electron mobility. For large grains ($D \gg \delta$) the sensing mechanism is controlled by the grain boundaries (Figure 2c). For ultra-fine nanoparticles (Figure 2d,e) there are two possible mechanisms as a function of the grain size (D). If the grain size is bigger than twice the Debye length of SnO_2 ($\delta \approx 3$ nm at 250 °C),[21] a conduction channel with bulk mobility exists within a diameter ($L_C = D - 2\delta$) from the grain center (Figure 2d). A change in the scattering center concentration (O_2^-, O^-, O^{2-}) will then only result in a change in the conduction-channel width (L_C). In contrast, if the SnO_2 grain is smaller or equal to twice δ then the whole grain is depleted (Figure 2e), therefore a reduction of the ionosorbed oxygen may "open" a conduction channel through the oxide (Figure 2b).

As "opening" the conduction channel increases the SnO_2 electron mobility remarkably and thereby its conductivity,[21,48] the response of SnO_2 sensors to a reducing analyte increases considerably when the grain size approaches 2δ (Figure 3a).[29,48] However, such small grains (ca. 6 nm) have high sintering rates at the operation temperature of SnO_2 semiconductor gas sensors (250–450 °C) and it is difficult to stabilize their size even below 10 nm (Figure 3b).[26] Therefore the expected increase in sensor response with decreasing grain size is only partially reached experimentally.[48]

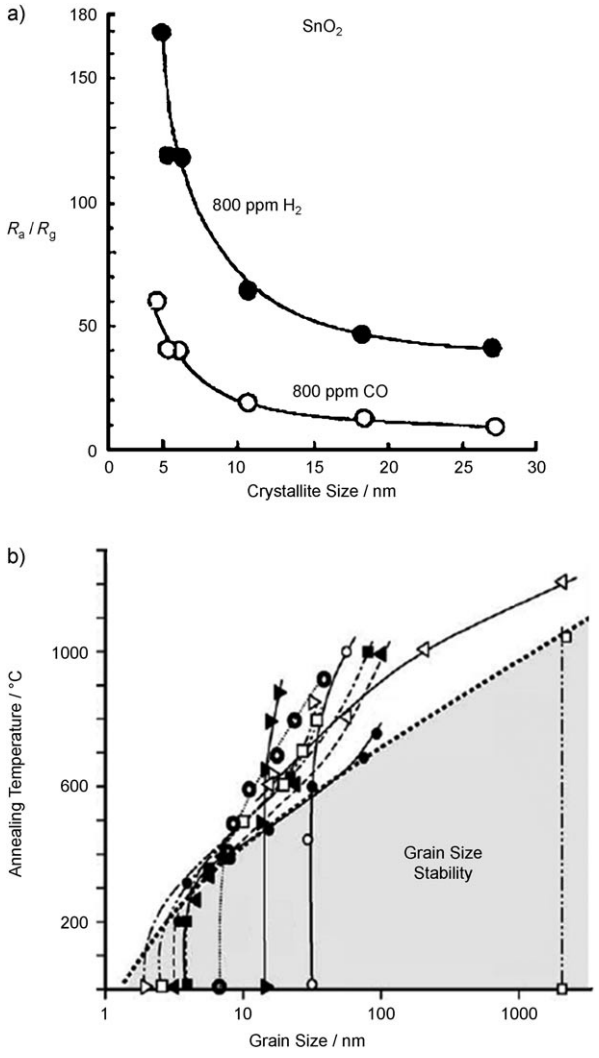

Figure 3. a) SnO_2 sensor signal (R_a = resistance in pure air and R_g = resistance with the analyte) to H_2 (●) and CO (○) at 300 °C as a function of the crystal size (adapted from Ref. [29]). The response increases steeply as the crystal size approaches two times the Debye length ($\delta = 3$ nm). b) Such small SnO_2 particles (different symbols and lines represent results obtained in various group) have a high sintering rate (even at moderate temperatures (adapted from Ref. [26]) and it is hard to obtain long-term, thermally stable, and highly sensitive grains of 6 nm.

3. Sensing-Film Morphologies

Classification of semiconductor films for gas sensors is based on their morphology and thereby sensing mechanism. In fact, although the interaction between a metal oxide semiconductor (e.g. SnO_2) surface and a reducing or oxidizing analyte is understandable along the oxygen-vacancy or ionosorption theory, the film morphology and its interaction with the sensor substrate also play an important role.[24]

Commonly, sensing films are subdivided in dense (compact) and porous.[24] In dense films, the gas interaction takes place only at the geometric film surface as the analyte cannot penetrate into the sensing film (Figure 4). In porous films, the gas can penetrate into the substrate and interact with single grains, sinter necks, and at the grain substrate/electrode interface.[24]

A general model of semiconductor, metal oxide gas sensors describing the sensing performance of various films is based on these two film categories.[24] Nevertheless, the simple distinction between dense and porous films is too coarse to describe all feasible morphologies. In fact, while several processes (such as spray pyrolysis) produce nanocrystalline metal oxide films with a certain overall porosity, their grain and crystal properties are not homogenous throughout the film,[26] therefore "dense" and "porous" regions coexist in the same "porous film". In contrast, novel methods, with decoupled particle synthesis and film deposition, such as flame spray pyrolysis (FSP),[50] produce fully porous films without dense regions. With respect to this distinction, at this point, a new class of "particulate" sensing films, obtained from deposition of solid nanoparticles (and only moderate substrate and sintering temperatures) is introduced (Figure 4).

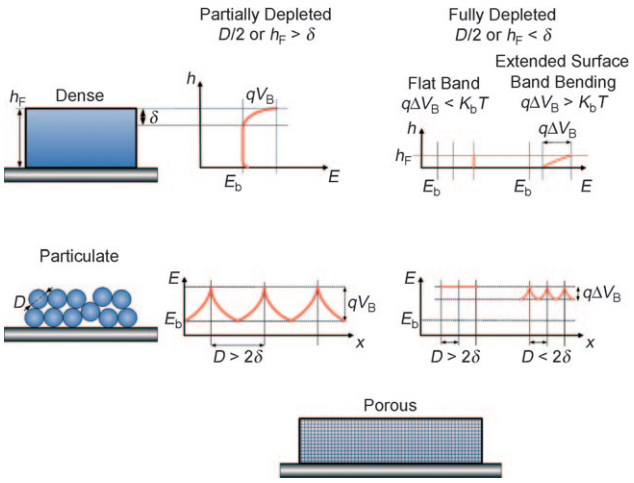

Figure 4. Schematic representation of geometry and corresponding energy band for dense, particulate, and porous films (adapted from Ref. [24]); where δ is the Debye length, D is the grain size, h_F is the film thickness, q is the elementary electron charge, V_B is the grain boundary potential, E_b is the bulk band energy, K_b is the Boltzmann constant, and T is the material temperature. The ionosorption of oxygen on the metal oxide surface forms surface barriers, with a height equal to qV_B, which bends the oxide energy band within the Debye length reducing the oxide conductivity. For partially depleted dense or particulate films, $D/2$ or $h_F > \delta$, a conduction channel where the band energy corresponds to that of the bulk is still available. For fully depleted dense or particulate films, $D/2$ or $h_F < \delta$, the bulk band energy, E_b, is not reached and the conductivity of whole material is reduced. Furthermore, if the energy barrier height, qV_B, is smaller than the thermal energy, K_bT, the energy band can be considered flat, otherwise a partial bending toward the surface remains. The contribution to the sensitivity of a porous film, containing particulate and dense regions, is composed of all possible combinations of the constituents. For further details, see Refs. [1, 24].

3.1. Dense Films

Completely dense films are not commonly used for semiconductor gas sensors, this is because the number of sites available for interaction with the analyte increases with increasing exposed metal oxide surface and thus with film porosity.[3,26] Nevertheless, they can be considered as the limit for high-temperature sintered (nearly melted) porous films or regions of porous films. Furthermore, the sensing properties of SnO_2 dense films made by atomic layer deposition (ALD)[71,72] and molecular beam epitaxy (MBE)[73] have been tested recently. Figure 4 shows a schematic representation of the energy band of a dense film in air. The ionosorbed oxygen atoms scatter electrons within the Debye length (δ), thus, to obtain high sensitivity, the thickness (h_F) of a dense film should be similar to δ (Figure 4, fully depleted). To fulfill this requirement extremely thin films (ca. 3 nm for SnO_2 at 250 °C)[21] are needed, however this leads to high sensor resistances and poor mechanical stability. In contrast, if the film is partially depleted (Figure 4) only a fraction of the film is affected by the reaction with the gas and therefore a moderate response is expected.

3.2. Particulate Films

An ideal semiconductor gas detector could consist of a single metal oxide particle with a grain size less than twice the Debye length. Nevertheless, such an ideal system cannot be realized easily and commercialized at low cost, to date. Instead, particulate films consist of several nanoparticles forming a network (Figure 4) that bridges between the measuring electrodes. The exact contribution of grains, necks, agglomerate and aggregate boundaries, particle–substrate and particle–electrode interfaces to the total sensor response is not trivial.[24] On the other side, for ultra-fine particles ($D \leq 10$ nm) it is known that the depletion of the grain and neck surfaces (Figure 2d,e) play the main role in determining the response to an analyte.[21,24,48]

Figure 4b shows a schematic representation of the band bending of a particulate film in air. In agreement with the ionosorption theory, a distinction between partially and fully depleted conditions is made. The main advantage in comparison to dense films is that it is not necessary to decrease the film thickness down to the Debye length of the oxide to reach high sensitivity. As the interaction between gas and oxide surface takes place on each grain, all the sensing material (with some exception for thick films) participate in the detection mechanism. In this way, both high sensitivity and reasonable resistances are feasible by controlling the film

thickness and the grain size separately. Such films are usually obtained by wet-deposition of pre-synthesized particles,[47] but recently some aerosol methods, such as FSP, have achieved similar results with higher uniformity of the film morphology.[50,74]

3.3. Porous Film

Porous film morphologies are the most common for semiconductor gas sensors. They can be obtained by several methods and are usually the result of limited control over the grain morphologies during deposition or post-deposition sintering/annealing. In fact, although several methods, such as spray pyrolysis,[26] pulsed laser deposition,[75] and sputtering,[28] can produce semiconductor films with relatively good control of single properties, only a few can control independently film thickness, grain, and crystal size. Therefore a porous film contains multicrystalline grains which act as dense films and monocrystalline grains which act as a particulate film (Figure 4c). The sensitivity of such porous films towards an analyte and the optimal thickness of such a film depends on the respective fractions of dense and particulate components. This situation is in agreement with the variations in sensitivity, operation temperature, and film thickness reported in literature for the same materials and the same synthesis processes (Table 1).

3.4. Film Thickness

The effect of film thickness on the sensing properties of a perfectly dense film is qualitatively simple. Increasing film thickness decreases the sensor response as the fraction of material involved in the interaction with the analyte is monotonously decreased (Figure 4a).[76] This situation however, is not always the case for porous or particulate morphologies[77] (Figure 5) as the analyte can penetrate into the film.[47]

For an isothermal porous or particulate film two main effects are distinguishable with increasing thickness: an increase of the total available surface for interaction with the gas and thereby of its overall reception function and, as result of the oxidation or reduction reactions, a decrease in the gas concentration at the bottom of the film. The effect of increasing film thickness is not trivial, as an increase in the gas reception sites does not result in a linear increase of the sensor response and the decrease of the gas concentration in the film varies with material, porosity, temperature, catalytic activity, and analyte composition.

To some extent a porous/particulate film can be modeled as a network of parallel and serial resistive elements (R_{nm}) extending between two measuring electrodes (Figure 5, bottom).[47] In this way the gas concentration profile is considered by computing the reaction between gas and each resistive element as a function of the coordinates in the film. The total sensor response is then calculated by the change in corresponding total resistance.[47] Despite the strong assumptions made in the model, it was shown that too thick films can decrease the sensor response by combusting the gas in the upper layer of the film,[47] therefore an optimization of the film thickness is necessary to maximize the sensor response.

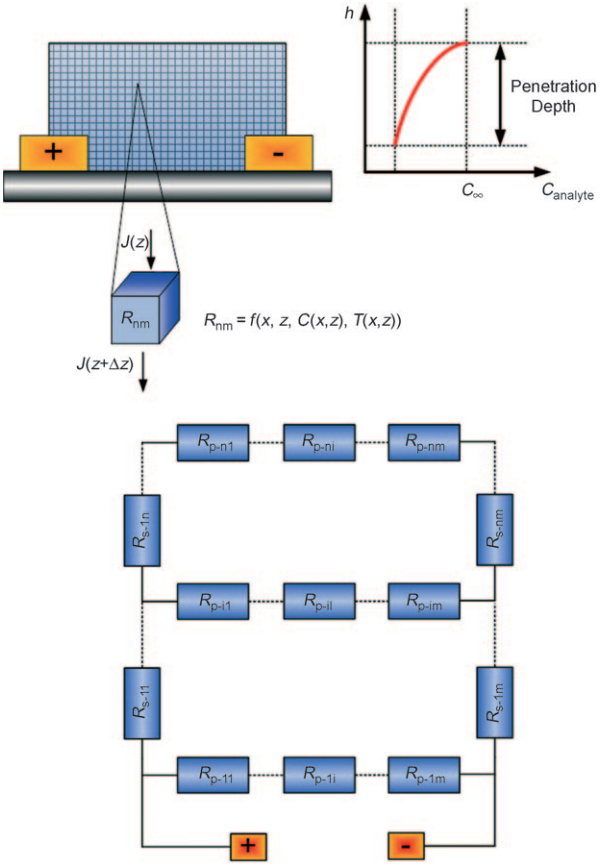

Figure 5. Top left and bottom: Schematic representation of a porous (or particulate) film as a network of parallel and serial resistive elements (R_{nm}) extending between two measuring electrodes (adapted from Ref. [47]). Each (grain or) resistive element has different response to the analyte as its concentration ($C(x,z)$) is reduced while penetrating into the film (top right). For non-isothermal films the different temperatures ($T(x,z)$) of the resistive elements must be considered. J = analyte mass flow.

4. Sensing-Film Synthesis

4.1. Dry and Wet Methods

A first distinction between semiconductor gas sensors was made for thin[10] and thick films.[11] Originally, this classification did not differentiate only the thickness of a sensing film, but also the synthesis method with the aerosol- and the wet-route producing thin and thick films, respectively.[47] As briefly discussed, the gas detectors introduced by Seiyama[10] consisted of ZnO thin films 20–100 nm thick which were made by vacuum evaporation of metallic zinc and subsequent oxidation at 450 °C. These first dry-made films (Figure 1a) were highly sensitive to several analytes, such as toluene, benzene, ethyl ether, ethyl alcohol, propane, and carbon dioxide,[10] but they had poor long-term stability and their

Table 1: Aerosol methods for synthesis of semiconductor films and corresponding sensor responses.

Process (abbreviation)	Film Structure[a]	Material	Response ($R_{air}/R_{gas}-1$) to gas (ppm) EtOH	H_2	CO	Ref.
Atmospheric Pressure Chemical Vapor Deposition (ACVD)	D/PO	F:SnO_2				[97]
		SnO_2		0.04 (300)		[98]
		SnO_2			0.6 (10^3)	[105]
Atomic Layer Deposition (ALD)	D	SnO_2			0.25 (10^4)	[71]
		SnO_2			2.3 (250)	[106]
		SnO_x			43 (5×10^4)	[76]
Combustion Assisted Chemical Vapor Deposition (CCVD)	PO	SnO_2	279 (100)			[74]
Direct Current Sputtering (DC-SPU)	D/PO	Pd:SnO_2	0.43 (3×10^3)	0.18 (3×10^3)		[4]
Evaporation (EVP)	D/PO	SnO_2				[21]
		SnO_2	1 (3.2×10^3)			[107]
Flame Spray Pyrolysis (FSP)	PA	SnO_2	5.3 (10)		4 (50)	[50]
		SnO_2	20 (10)			[32]
			45 (50)			
		Si:SnO_2	50 (10)			[32]
			318 (50)			
		Pt:SnO_2			0.8 (10) at 50% r.h.	[50]
		Pt:SnO_2			3.4 (10) at 25% r.h.	[51]
Hot Wall Aerosol Reactor and Low-Pressure Impactor (HWLP)	PA	$SnO_{1.8}$	3 (10^3)			[39]
		Ag:$SnO_{1.8}$	39 (10^3)			[39]
Ion Beam Sputtering Ion Assisted Deposition (IAD)	D/PO	SnO_x		3.8 (100)		[108,109]
		SnO_2		18 (400)		[110]
		SnO_2	6 (10^4)		4 (10^3)	[111]
		WO_3	1.5 (10^4)		0.5 (10^3)	[111]
Molecular Beam Epitaxy (MBE)	D	SnO_2	1.8 (100) @ 40% r.h.	3.7 (10^3)		[73]
Organometallic Chemical Vapor Deposition (OMCVD)	D/PO	SnO_2	8 (100)			[87]
		SnO_2			0.53 (10)	[95]
Plasma enhanced Chemical Vapor Deposition (PECVD)	D/PO	SnO_2	40 (10^3)	100 (10^3)	22 (10^3)	[86]
		Pd:SnO_2	14 (50)	32 (50)	1 (50)	[86]
		SnO_x	17 (50)			[94]
Pulsed Laser Deposition (PLD)	D/PO	SnO_2	6 (50)			[75]
		SnO_2		10 (10^3)		[112]
		SnO_2			4.5 (50)	[89]
Radio Frequency Sputtering (RF-SPU)	D/PO	SnO_x	1.5 (100)			[113]
		SnO_2			0.18 (100)	[114]
		SnO_2			0.5 (150)	[115]
		SnO_2		300 (10^4)		[116]
		SnO_2		2.3 (10^3)		[58]
		Pd:SnO_2		4470 (10^3)		[58]
Rheotaxial Growth and Thermal Oxidation (RGTO)	PO	SnO_2	21 (10^3)	41 (100)	1 (10^3)	[28]
		Pd:SnO_2	60 (10^3)	90 (100)		[62]
		SnO_2			0.3 (100)	[117]
		SnO_2		0.1 (600)		[85]
		Ti:SnO_2		4 (10^3)		[118]

Table 1: (Continued)

Process (abbreviation)	Film Structure[a]	Material	Response ($R_{air}/R_{gas}-1$) to gas (ppm) EtOH	H_2	CO	Ref.
Supersonic Cluster Beam Deposition (SCBD)	PA	TiO_2	35 (500) Methanol			[78]
Spray Pyrolysis (SP)	D/PO	SnO_2	2.3 (3200)			[107]
		SnO_2		0.04 (300)		[98]
		SnO_2		10^3 (2×0^4)		[77]
		SnO_2			24 (5×10^3)	[88]
		Pd:SnO_2			104 (5×10^3)	[88]

[a] D: dense, PO: porous, PA: particulate.

sensing response decreased gradually to two thirds in eight months.[16]

This poor long-term stability was attributed to their thickness, which caused mechanical and especially "electrical" fragility,[11] therefore a new wet method for the synthesis of thick sensing films was proposed. The thin film was substituted by a "…*main sensitive body consisting of metal-oxide semiconductor material*…" as "…*a block or thick layer formed by compression forming, sintering or brushing with a suspension of powdered semiconductor material in a suitable medium*".[11] In praxis, this block or film was made either by deposition and sintering of a paste/solution containing semiconductor grains[29] or by direct sol–gel synthesis on the substrate (Figure 6).[30]

Sensing films made by wet methods have particulate morphology (Figure 4), but also porous films are possible if elevated calcination/sintering temperatures are applied.[47] They are classified still as thick-film sensors, as it is technically challenging to decrease the thickness of wet-made films below 1 μm while preserving their contiguity.[47] Although particulate film morphologies have often the highest sensor response,[24,48] wet methods offer only limited control over film porosity and thickness. These issues limit the maximization of the sensor response as a function of film thickness. The reproducibility of wet-film morphology is poor because of crack formation during the evaporation of the binders and solvents and thereby conspicuous variations between sensor performances are common.[50] Furthermore, wet methods are multistep processes (Figure 6) that often require long production time because of the evaporation and sintering/calcination steps.

In contrast, dry methods offer an interesting possibility for the rapid synthesis of semiconductor sensing films (Figure 6) and have overcome several of the initial shortcomings associated with their use.[26] Most of them tend to produce porous or nearly dense films (Figure 4) and have thicknesses under 1 μm, and therefore are classified as thin-film sensors.[47] Nevertheless, novel aerosol methods, such as aerosol synthesis and deposition of sensing nanoparticles,[50] produce particulate morphology with variable film thickness (100–10^5 nm). Therefore, their classification extends over the old "thin" and "thick" nomenclature and they represent an extension of the "thick" particulate film morphology in a "thin" film.

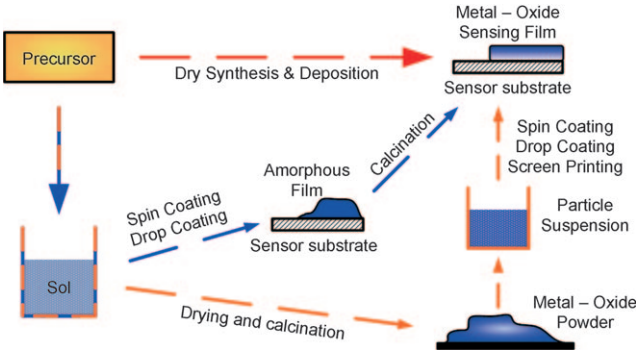

Figure 6. Schematic of dry (top red arrow) and wet (orange and blue arrows) synthesis of metal oxide films for semiconductor gas sensors. Several dry processes can give synthesis and deposition of the crystalline metal oxide films in one step. In contrast, wet methods (such as sol–gel) require multistep processes with long evaporation and annealing/calcination times.

4.2. Rapid Dry Synthesis

Since the fabrication of the first semiconductor gas sensors, several dry methods have been applied to the

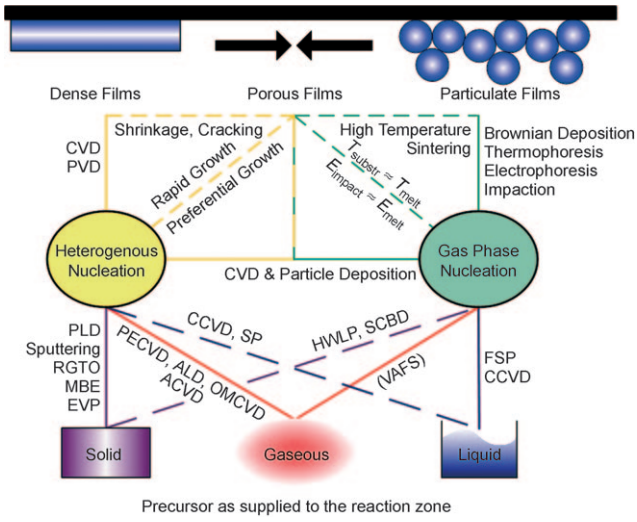

Figure 7. Typical dry methods and pathways for the synthesis of dense, porous, or particulate film morphology in which solid, gaseous, or liquid precursors are supplied to the reaction zone. The method in parenthesis is uncommon for semiconductor gas sensors (for abbreviations see Table 1).

synthesis of metal oxide films.[62] As discussed above, such classical methods produce mainly thin films with some degree of porosity,[62] but this is not always the case. In fact, completely dense or extremely porous (>98%) particulate films have been fabricated recently by ALD[71] and FSP,[50,51] respectively. This control over film morphology and the feasibility of one-step synthesis (Figure 6) of simple and complex metal oxide films[3] extends far beyond the options offered by wet methods.[26]

Figure 7 shows a schematic (abbreviations reported in Table 1) of common methods and pathways for the dry synthesis of dense, porous, and particulate films starting from solid, gaseous, or liquid precursors. A first distinction is possible between methods based on heterogeneous nucleation on the substrate surface[62] and those based on homogeneous nucleation in the gas phase (Figure 7). The heterogeneous nucleation on the substrate surface is required for the synthesis of perfectly dense films, where growth is obtained either by chemical or physical vapor deposition.[62] Classical methods are sputtering, atmospheric-pressure chemical vapor deposition, and spray pyrolysis,[62] but several others are possible (Figure 7 and Table 1). The average porosity of such films is controlled by several parameters, such as process pressure, substrate temperature, and precursor feed rate, but it is often difficult to obtain homogeneous films and a distribution of particulate and dense film regions is common (Figure 4).[26]

In contrast to physical and chemical vapor deposition processes, homogeneous nucleation in the gas phase leads to particle formation and growth. These particles can be deposited directly from the aerosol to the substrate surface (Figure 7) by Brownian deposition, thermophoresis,[50] electrophoresis,[53] and impaction.[39,78] In absence of restructuring, which could arise from high substrate temperature or impaction energy, the resulting film consists of the particles produced in the gas phase and thus has a homogeneous composition and morphology.[50] With respect to the sensing properties, such films can be classified as particulate (Figure 4) and, if sufficiently small particles are deposited, produce highly sensitive sensors (Table 1).[21,24,48] Post-annealing of these particulate films causes sintering and grain growth resulting in porous films. Nevertheless, it is doubtful if fully dense films are achievable, without melting the metal oxide, as disintegration occurs before.[79] Some methods, such as vapor-fed aerosol flame synthesis (VAFS: Figure 7) are also able to produce semiconductor nanoparticles of controlled size and crystallinity[80] but to date have not been utilized for direct deposition of sensing films.[81–83]

4.2.1. Process Design

The required maximal substrate temperature (T_s) and minimal pressure (P_{min}) during film growth or post-treatment are important parameters for process design. Figure 8 shows a

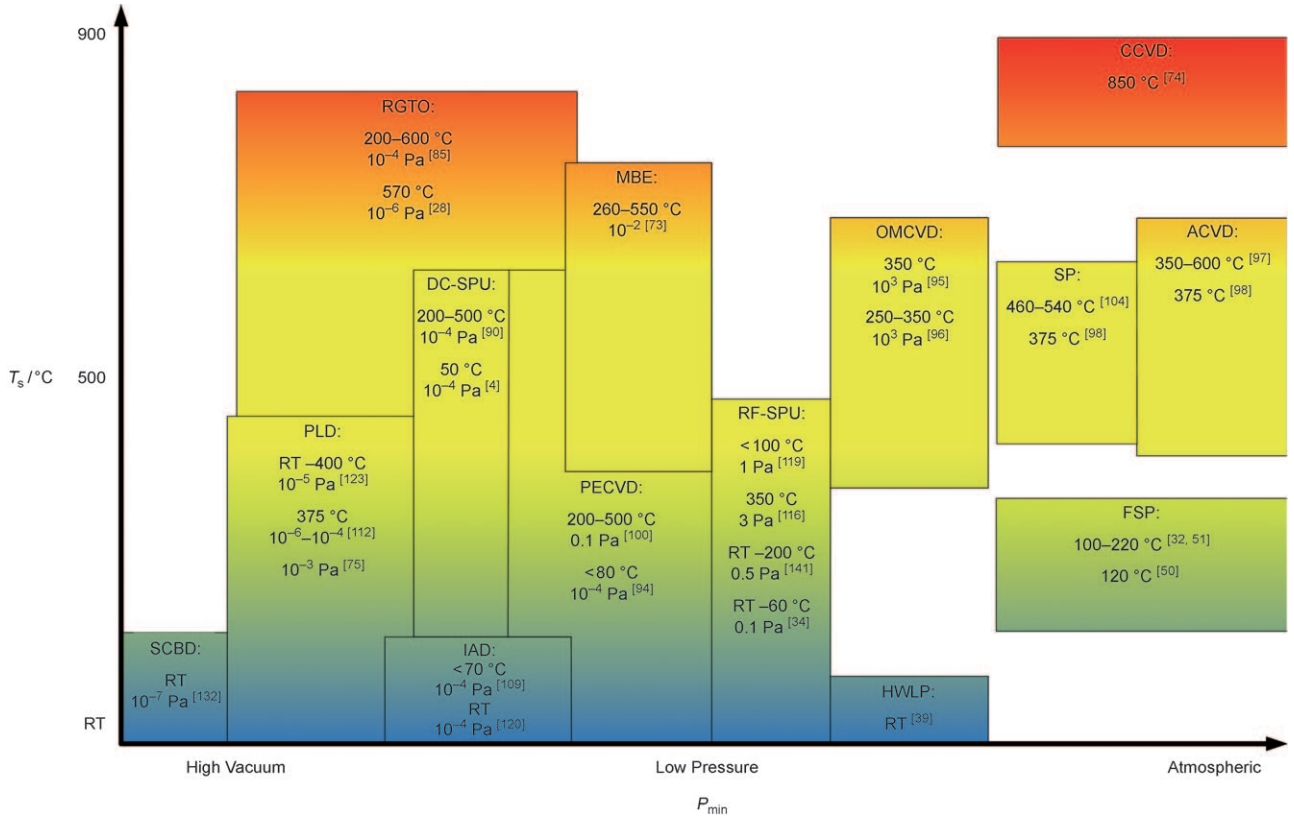

Figure 8. Examples of dry processes utilized for the synthesis of gas-sensitive nanostructured films arranged by minimum process pressure (P_{min}) and maximum substrate temperature (T_s). Several processes are able to deposit at room temperature, however, post-annealing is often necessary to obtain fully crystalline films. The indicated pressures and temperatures are only guidelines as a broad range of process conditions are possible.

selection of dry methods with corresponding process conditions utilized for the synthesis of nanostructured films for semiconductor gas sensors. As will be discussed in Section 4.3, a large variety of process parameters are possible within the same method and (Figure 8) the reported conditions are only indicators. In general, atmospheric methods have the advantage of easier scalability and lower process cost than vacuum-based processes (P_{min}: Figure 8) as no expensive evacuating systems are required. Low substrate-deposition temperatures (T_s: Figure 8) are often necessary for deposition on devices with integrated circuitry, such as CMOS-based micro-gas-sensors.[18,84] Several dry processes are able to deposit the nanostructured film from moderate down to room temperatures (Figure 8), however, annealing/calcination is often required to obtain fully crystalline materials and conducting films. For example, it was observed that a post-annealing/oxidation step with a temperature of at least 570 °C is necessary to obtain a continuous electrical path in RGTO-made SnO_2 films.[28] Furthermore, synthesis of high-performing sensing films requires optimization of these process conditions as observed for spray pyrolysis[26] and therefore operation is often limited to a narrow window of temperatures and pressures. In fact, low pressure promotes film densification and high substrate temperature grain growth. A correct choice of both parameters can lead to significant increase in sensor response and selectivity to specific analytes as accurately pointed out for (magnetron) sputtered SnO_2 films.[58]

4.3. Chemical and Physical Vapor Deposition of Dense and Porous Films

Several methods for the chemical and physical deposition of SnO_2 films have been reviewed previously.[62] In general, the sensing properties of such thin films can vary greatly (Table 1). For example, the response of SnO_2 RGTO-made films (Table 1) to H_2 can be 41 at 100 ppm[28] or 0.1 at 600 ppm.[85] (Sensor response have in general no units as they are the ratio between resistance in air and with the analyte.) The response of PECVD-made SnO_2 films to 1000 ppm EtOH reaches 40[86] while the response to 100 ppm EtOH of an OMCVD-made film is barely 8.[87] This result is not surprising and it is attributed to the large spread of porosities, grain and crystal sizes, film thicknesses, and morphologies (porous and dense).[26] As discussed above, all these properties have a strong influence on both sensor reception and transduction functions. In fact, it is possible to produce sensing films by CVD or PVD deposition, with a performance as high as the ones made by CCVD,[74] SP,[88] RGTO,[28] and PLD[89] (Table 1), but it is often necessary to find the perfect set of process parameters experimentally. This task is even more challenging as often porosity, grain and crystal size are correlated and change during film growth or post-processing (annealing).[26,90]

In this context, novel synthesis methods, such as electrodeposition, may show interesting results in the future. Electrodeposition has been utilized recently for the synthesis of nanostructured semiconductor thin films.[91,92] Several semiconducting oxides (e.g. ZnO, TiO_2) with bandgaps ranging from few to several eV have been synthesized already. Among these, zinc oxide has been the subject of the majority of studies because of its wide range of applications,[93] such as transparent conducting oxide (TCO), sensors, light emitting devices, lasers and transistors. Electrodeposition appears promising also for application in the synthesis of metal oxide gas sensors because of its precise control on the resulting film morphology.

4.3.1. Chemical Vapor Deposition

Chemical vapor deposition is a powerful method for the synthesis of dense or porous (Figure 4) nanostructured films. In general, a gaseous precursor (Figure 7) is supplied to the reaction zone and synthesis of the final products (metal oxides) takes place directly on the target substrate. In the last few decades several CVD variations have been developed allowing deposition from low (PECVD,[94] OMCVD[95,96]) to atmospheric (ACVD,[97–99] CCVD[74]) pressures (Figure 8). A minimum substrate temperature (> 300 °C) is often necessary to complete reaction/oxidation of the precursors.[95,96,98] However, also deposition at nearly room temperature is possible by utilization of more elaborate systems, such as plasma enhanced CVD.[94]

A large variety of film morphologies (Figure 9) and corresponding sensing performances are possible by choosing the appropriate deposition method and process conditions.

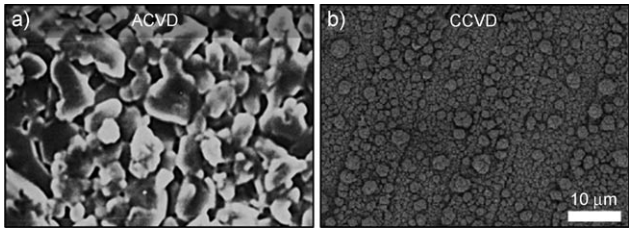

Figure 9. SnO_2 film morphologies obtained by a) ACVD[97] and b) CCVD.[95] The fine grains obtained by CCVD (b) result in high sensor response to EtOH (Table 1) while the coarse ACVD films (a) have poor sensitivity toward several analytes (e.g. H_2 and CO).

Nevertheless, synthesis of semiconductor sensing films by classical CVD processes (e.g. ACVD,[97] OMCVD[95]) has resulted in poor sensor response to several analytes (Table 1). This could be attributed to the predisposition of such methods to produce dense films (or gas-tight multicrystalline domains) and this insufficiently depleted grains (Figure 4).

The sensor responses can be increased remarkably utilizing novel CVD-based processes such as PECVD[94,100] and CCVD[74] which can produce smaller grains that are better accessible by the analyte (Table 1). For example, in PECVD processes, tailoring of the film, and to some extent, of the grain properties is possible, not only by process pressures and temperatures,[101] but also by varying deposition time, substrate distance, and radio-frequency (RF) power.[102] However, gaining an understanding of the film growth mechanisms

of some of these methods is still in progress. In CCVD, for example, a SnO_2 liquid precursor is sprayed and combusted in the proximity of a substrate heated at high temperature (> 800 °C).[74] This method is also utilized for the gas-phase synthesis of SnO_2 nanoparticles[50] and it is therefore difficult to differentiate between heterogeneous nucleation on the substrate surface and homogeneous nucleation in the gas phase.[74] The resulting film morphology (Figure 9) is most probably a combination of both film synthesis processes and therefore the control over its properties is challenging.

4.3.2. *Spray Pyrolysis*

Spray pyrolysis (SP) has been widely applied for the synthesis of semiconductor gas sensors. An extensive Review linking film structural properties and sensing performance has been published recently.[26] The grain shape is controlled by deposition temperature and film thickness and thereby tailoring of analyte-specific adsorption sites is possible.[77,103] In particular, the substrate temperature is a delicate parameter as it influences droplet vaporization or pyrolysis, precursor oxidation, sintering, and crystal growth.[103]

As observed above for other CVD-based deposition methods, a main issue is the limited control over the analyte penetration into the film and thus the grain accessibility. In most studies only the crystal size is reported because of technical difficulties in determining the grain size based on the accessible surface.[104] This situation is particularly aggravating as in SP-made films the grain size can be more than three-times the visible grain size observed by SEM.[88] As a consequence, the interpretation of the sensing response based on the size determined by X-ray diffraction data is sometimes misleading (Figure 4).[104]

Figure 10 a–c shows the morphological evolution, and the corresponding sensing properties are shown in Figure 10 d, of SP-made SnO_2 thin films as a function of film thickness (δ_{Film}).[77] Increasing the film thickness from 37 to 300 nm increases drastically the visible (SEM) grain size (Figure 10 a–c).[77] The increase in grain size suggests that the gas sensitivity should decrease with increasing film thickness (Figure 4).[24] Nevertheless, after a minimum at about 50 nm the sensitivity (Figure 10 d) increases with increasing thickness. This result is in agreement with the complex modeling of the sensor response for porous films and depends also on the molecular composition of the analyte and the film operating temperature.[47]

4.3.3. *Sputtering*

Physical vapor deposition of semiconductor gas-sensor films by sputtering-based processes is particularly interesting when suboxides[119] or specific crystal-plane orientations[116] are desired. A relative good control over the film morphology is possible ranging from porous to nearly pin-hole-free, dense films. Specific crystal-plane orientations are obtained by tuning the substrate properties.[116] Furthermore, the substrate can be kept at room temperature during deposition.[113]

Main short-comings are the necessity to operate at low pressure and the poor crystallinity[116] when operating at low

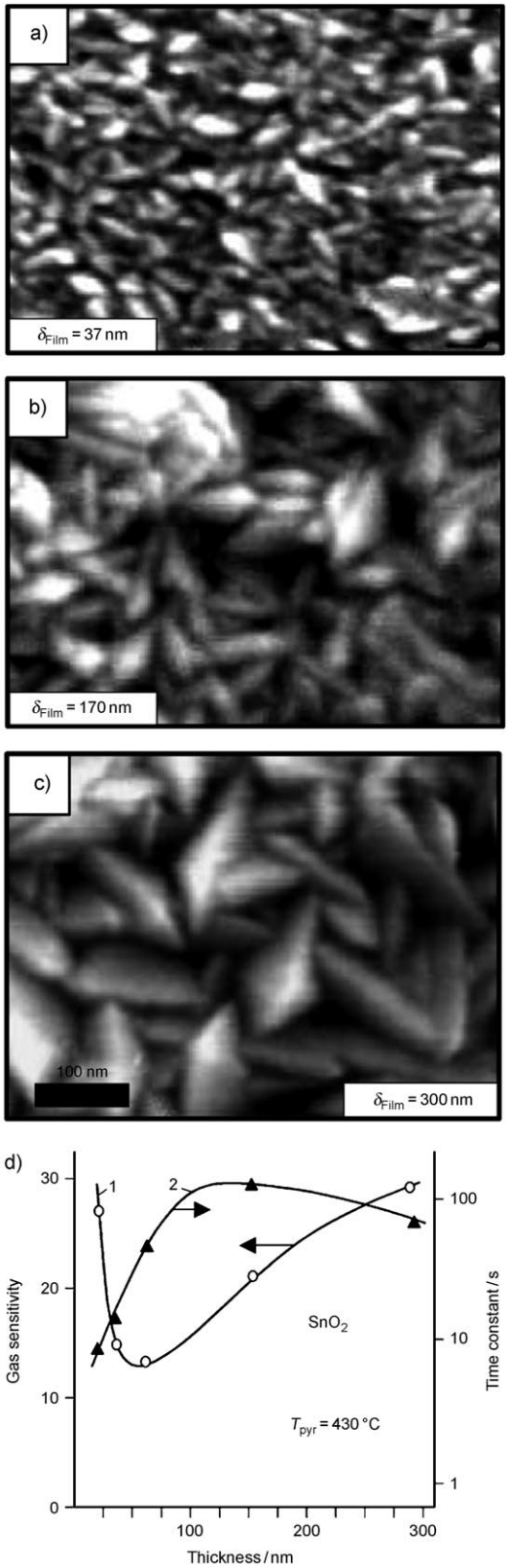

Figure 10. Characterization of SP-made SnO_2 thin film morphologies (a–c; scale bar applies to all three images) and sensing properties (d) as a function of the film thickness (δ_{Film}).[77] The grain size increases drastically with increasing film thickness (a–c). A minimum in gas sensitivity is reached around δ_{Film} = 50 nm and then increases with increasing thickness (d); 1, ○ = gas sensitivity; 2, ▲ = time constant.

substrate temperature. In fact, post-annealing from moderate to high temperatures (e.g. 400[113] and 600 °C[116]) is necessary to obtain fully crystalline material. Furthermore, synthesis of tin oxide films often results in formation of both Sn^{4+} and Sn^{2+} valence states[119] and thus reduced sensitivity.[113,119]

Both classical RF[113] and DC[4] magnetron sputtering have been utilized for synthesis of SnO_2 sensing films, however, the sensor responses vary between poor and moderate (Table 1). The film performances are slightly better utilizing ion-beam sputtering[120] or ion-assisted deposition (IAD).[109] Nevertheless, they are generally worse than that of standard wet-based deposition processes (e.g. screen printing).[113] As discussed above, this is partially attributed to the co-synthesis of Sn^{2+} which is less gas-sensitive than Sn^{4+} but also the grain size plays an important role.[113] Indeed the extent of grain growth during deposition or post-annealing is poorly controllable (Figure 11).[120] Post-annealing temperatures above 600 °C

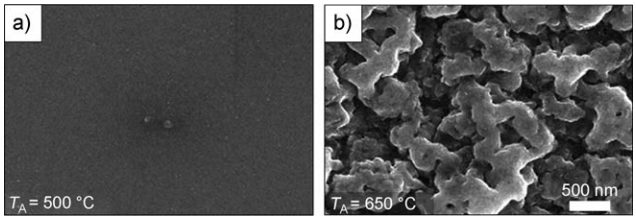

Figure 11. SnO_2 films obtained by ion beam sputtering post annealed at a) 500 and b) 650 °C (scale bar applies to both images).[120] To obtain fully crystalline SnO_2 films post-annealing temperatures (T_A) above 600 °C are necessary. However, this results in large dense (gastight) multicrystalline domains and thus poor sensor response.

(Figure 11 b) are required to obtain fully crystalline SnO_2 IAD-made films.[120] Nevertheless, this changes the film morphology dramatically (Figure 11) and has consequences for its sensing performance. After annealing at 650 °C, large grains of 500 nm are visible (Figure 11 b), but the crystal size is only 15 nm[120] suggesting formation of dense multicrystalline domains that cannot be penetrated by gas. In fact, the sensor response to 5000 ppm CH_4 is small and reaches barely 0.8.[120]

A better control over the final grain size is obtained by two-step physical vapor deposition/oxidation methods, such as RGTO.[28] First, a metal film (e.g. Sn by RF-SPU) is grown on a substrate kept at temperatures above the metal melting point (e.g. 232 °C for Sn). Thereafter, this film is oxidized forming the target oxide (e.g. SnO_2).[28] A minimum oxidation temperature (e.g. 520 °C) is necessary to obtain full phase transformation and electrical continuity between the grains.[28] Initially, high/moderate responses to H_2 have been reported for RGTO-made SnO_2 films (Table 1) and deposition of dispersed Pd nanostructures on the film was utilized to increase its sensitivity further.[62] The relatively small size and accessibility of the grains makes it an attractive method for the synthesis of semiconductor gas sensors for several analytes (e.g. CO and NO_x).[121] Furthermore, the sensor response (e.g. to NO_2) can be increased by optimizing the deposition temperature and thus the substrate surface coverage of Sn droplets.[122] Integration of RGTO-films in micromachined sensor substrates and deposition of Au nanoparticles over the SnO_2 film (Figure 12) has led to successful detection of C_6H_6 and NO_2 in the ppb range.[14]

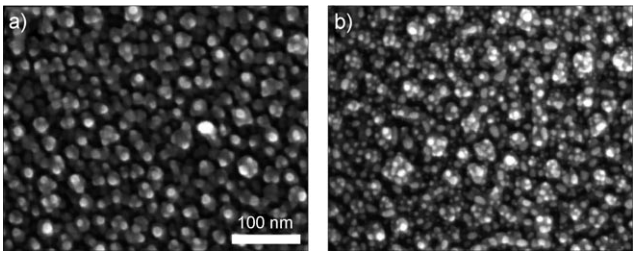

Figure 12. SEM images of RGTO-made SnO_2 films a) without and b) with Au nanoparticles (scale bar applies to both images).[14] The accessibility and small size of the SnO_2 grains (a) and the good dispersion of the Au nanoparticles (b) allow detection of analytes (e.g. C_6H_6, NO_2) in the ppb range.

4.3.4. *Pulsed Laser Deposition*

Synthesis of semiconductor gas sensor films by pulsed laser deposition (PLD; Figure 8) has shown promising results (Table 1) for some analytes, such as ethanol[75] and CO,[89] while only moderate response to others, such as H_2.[112] This situation could be attributed to the different conditions utilized in these studies as the film-growth dynamics of PLD is complex and highly sensitive both to growth (Figure 13) and

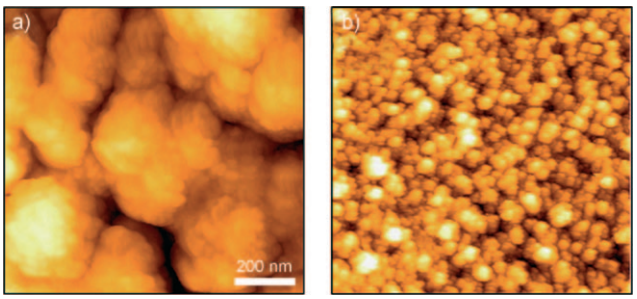

Figure 13. AFM images of PLD-made SnO_2 films deposited at a) room temperature and at b) 150 °C (scale bar applies to both images).[123] The accessible SnO_2 grain surface depends on the deposition conditions.

post-annealing steps.[123] PLD can produce fine grains (<10 nm) by control of the background oxygen pressure with moderate substrate temperatures (e.g. 300 °C).[89] However, the resulting crystal size is more than doubled by increasing the deposition temperature from 300 to 400 °C.[123] Deposition at room temperature is also possible but produces mainly amorphous phase, whereas fully crystalline SnO_2 films are obtained above 150 °C (e.g. 300 °C).[123] The accessibility of these grains (film porosity) to the analyte is not trivial to explain and depends on the deposition conditions (Figure 13). Integration of PLD-made SnO_2 films in micro-machined gas-sensor processes has been demonstrated recently.[112]

4.3.5. Molecular Beam Epitaxy

Investigation of the sensing properties of dense SnO_2 films (Figure 4) has been attempted by molecular beam epitaxy (MBE) with accurate control over film thickness and composition.[73] Poly- or monocrystalline films have been synthesized with the polycrystalline films having higher sensitivity than the monocrystalline ones. However, as expected (Figure 4) the sensor response to H_2 and ethanol are both extremely low (Table 1) as the films are too thick and dense and thus not completely electron depleted.

4.4. Particulate Film Assembly by Aerosol Synthesis and Deposition of Nanoparticles

Homogeneous nucleation of nanoparticles in the gas phase and their deposition from the resulting aerosol onto sensor substrates is a promising alternative to chemical or physical vapor deposition of nanostructured, metal oxide films (Figure 7). The main advantage is the separation of material and film synthesis steps. In contrast to what has been observed in CVD[77,97] and PVD[113,119] methods, grain and crystal properties can be tuned precisely[32,51] while maintaining sufficient porosity for the penetration of the analyte into the sensing film.

4.4.1. Film Growth Mechanism by Aerosol Deposition

The first step is the gas-phase synthesis of nanoparticles. There are several processes capable of producing well controlled nanosized metal oxide semiconductors including sputtering,[49,78] hot-wall aerosol reactors,[39,124] vapor-fed diffusion flames,[125–128] and liquid-fed spray flames.[32,45,50,51] Flame synthesis of nanoparticles bears the advantage of short process times, high scalability, and high particle concentration of the products.[129] Furthermore, utilizing spray flames an even larger number of material compositions are available with improved control over grain morphologies and dispersion.[65] Tailoring of the nanoparticles properties in

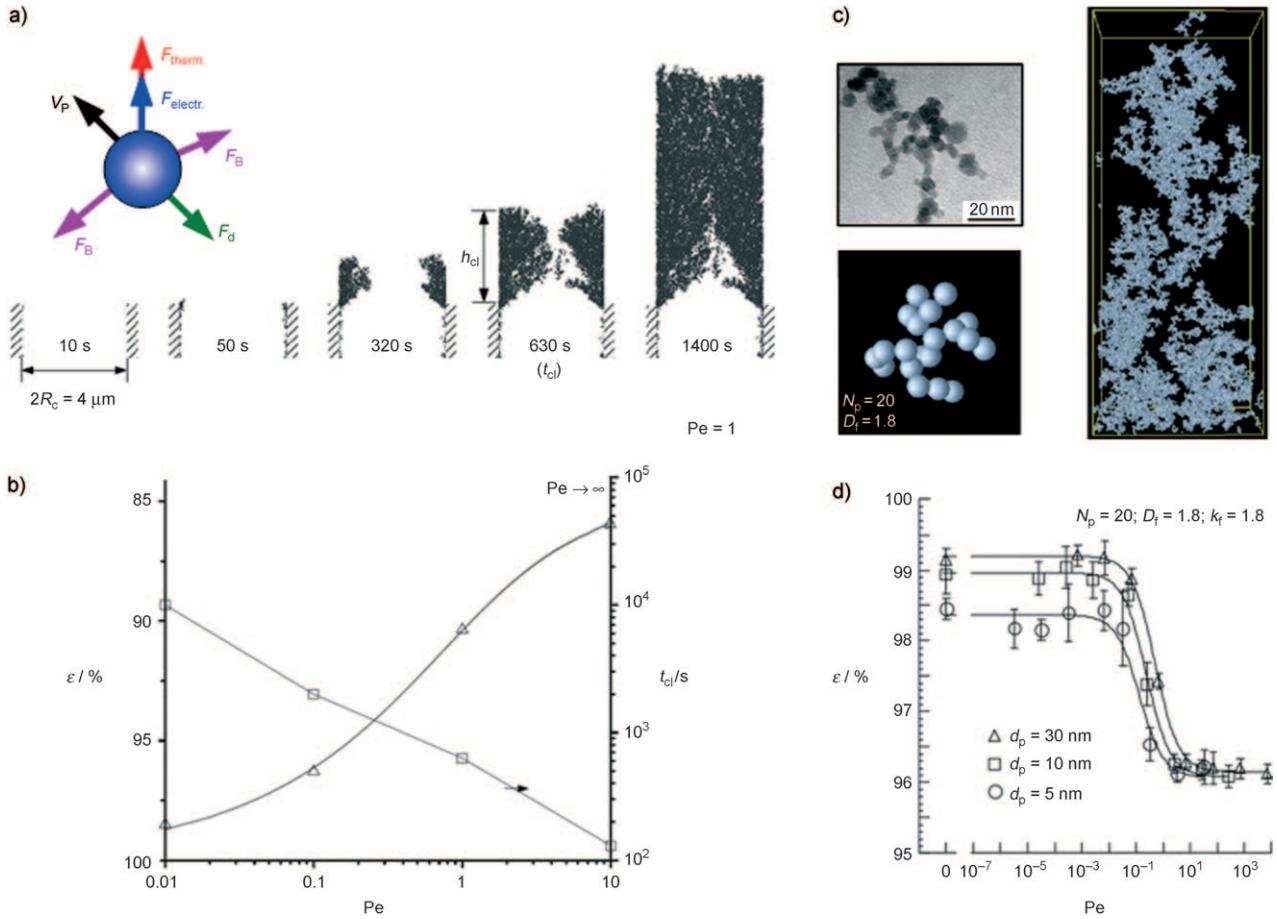

Figure 14. Film properties by deposition of single (a,b)[134] and agglomerated (c,d)[133] nanoparticles[13] as a function of the Peclet number (Pe); d_p = primary particle diameter, D_f = fractal dimension, N_p = number of primary particle in the agglomerate, k_f = fractal prefactor, R_c = capillary radius a) Nanoparticles approaching a surface with a velocity (V_p) experience several forces including a drag force (F_d) and a Brownian force (F_B). Application of a thermophoretic (F_{therm})[50] or electrophoretic (F_{electr})[53] gradient is utilized to increase the deposition rate or to produce precise patterns. Such deposition leads to the formation of continuous films even on porous substrates.[134] The resulting film porosity is determined by the Pe number (ratio of translational and diffusion velocity). At low Pe number (b) extremely high porosities (ε) are achieved (e.g. 98%) while at high Pe the minimum (ca. 85%) porosity is reached; t_{cl} = clogging time.[134] However, aerosols are often composed of agglomerated particles[133] and therefore even at high Pe only a minimal porosity of 96% is reached.

terms of grain size distribution,[39] aggregation,[130] crystal-plane orientation,[131] composition,[32] and shape[32] is possible directly in the gas phase.

The second step consists of deposition of nanoparticles onto the sensor substrate, and their self-assembly to a nanoparticulate film (Figure 4). The main deposition mechanisms (Figure 14a) depend on the aerosol conditions (e.g. velocity, pressure, temperature, particle size, and electrical charging) and include impaction,[39,132] electrodynamic forces (F_{electr}),[53] diffusion (F_B), and thermophoresis (F_{therm}).[50,51] The resulting film morphology (Figure 14a) is controlled by the ratio between translational and diffusion velocity (Figure 14b) of the nanoparticle (Péclet number, Pe).[133] Low film porosity (e.g. 85%) is obtained at high translational velocity (high Pe) for example in berner low pressure impactor (BLPI)[39,132] whereas high porosity (e.g. 98%) is obtained at low velocity as in thermophoretic driven deposition (e.g. FSP).[50,51] Although impactors have higher control over the translational velocity than thermophoretic-driven systems and thereby better control over the resulting morphology, they require low pressure (Figure 8, HWLP[39] or SCBD[132]) and the processes are more technically demanding than the thermophoretic-driven systems.[50,51] Aerosol deposition of nanoparticles (Figure 14b) leads to rapid formation of continuous films even on porous substrates.[134] Thus novel film layouts are feasible that go beyond those obtained by C/PVD methods. However, concentrated aerosols are often composed of agglomerated particles (Figure 14c). Deposition of such agglomerates leads to even higher porosity (Figure 14c) than that obtained by deposition of single nanoparticles. In fact, at high Pe number (Figure 14d, $Pe = 10^3$), it is hard to reach a porosity below 96% limiting the control over film morphology.[133]

4.4.2. *Flame Spray Synthesis of Particulate Films*

Flame synthesis of metal oxide nanoparticles has some advantage over other aerosol methods, as discussed in Section 4.4.1.[65] The temperature gradient between the hot flame fumes and a cooled sensor substrate can be utilized to increase the deposition rate by thermophoresis at atmospheric pressure (Figure 8).[50] Lately, the synthesis of SnO_2 semiconductor gas sensors has been investigated increasingly by flame spray pyrolysis (FSP).[32,50,51,135,136]

The as-deposited FSP-made films are highly porous (e.g. 98%) and consist of a lace-like network of the nanoparticles (Figure 15c,d) which have average grain and crystal sizes of approximately 10 nm thereby a nearly perfect "particulate" film is formed (Figure 4).[51] This arrangement allows penetration of the analyte into the film and depletion of all the grain surfaces (Figure 2). As a consequence, FSP-made films have a high sensor response (Table 1) to all tested analytes (e.g. EtOH, CO).[50,51] Furthermore, co-synthesis of SiO_2 allows tailoring of the sinter neck sizes and shapes so that fully depleted necks (Figure 2e) and ultrahigh sensitivities are obtained.[32]

The response of FSP-made SnO_2 films is comparable to those obtained by CCVD (Table 1). For both CCVD- and FSP-made sensors the responses to ethanol[50,74] and CO[50]

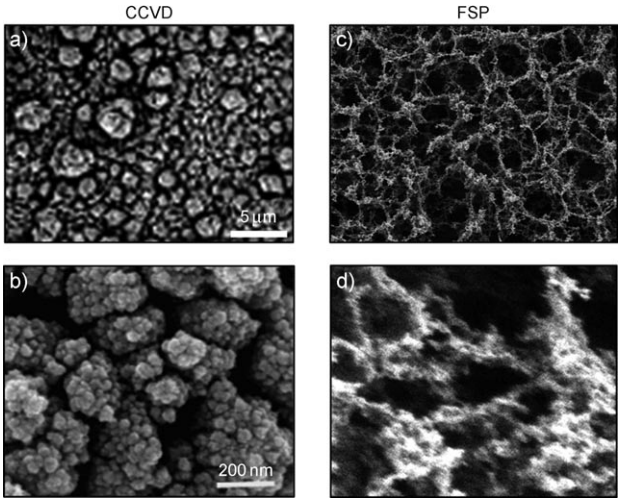

Figure 15. Comparison between a porous SnO_2 film obtained by CCVD[74] (a,b) and a particulate one made by FSP.[51] The film in (a,b) is obtained at high substrate temperatures (e.g. 850°C) by deposition of airborne particles and CVD on the substrate surface, whereas FSP-films are made at low temperatures (e.g. 120°C) by deposition of airborne particles.

were remarkably higher than that of films prepared by other dry methods (Table 1). This result was attributed to the small grain size (FSP: ca. 10 nm,[50] CCVD: under 30 nm[74]) and high porosity ($\varepsilon \approx 98\%$[50]) which are optimal properties for gas-sensing films.[24] Nevertheless, CCVD-films have a denser morphology (Figure 15a,b) than that of FSP-made ones (Figure 15c,d). In fact, CCVD produces porous (and not particulate) film morphologies (Figure 15b) by simultaneous CVD and particle deposition (Figure 7). Furthermore, a large amount of film restructuring is expected during CCVD deposition as the substrate temperature (e.g. 850°C) is kept above that required for the thermal stability of 10 nm grains (ca. 400°C, Figure 2e)[26] for a long time (e.g. 20 min).[74]

The similar sensor response of CCVD and FSP SnO_2 films (Table 1) is attributed to the film thickness not being optimized. Although CCVD sensors have been realized as thin films (e.g. 1 µm[74]), only thick (e.g. 30 µm) FSP sensors have been characterized to date.[32,50,51] As discussed in Section 3.4, the upper layers of a thick SnO_2 film may act as a catalytic filter drastically reducing the concentration of analyte reaching the rest of the film (Figure 10).[47] This situation was also reported for FSP-made $Pd:Al_2O_3$ films deposited on top of FSP-made SnO_2 films.[136] To have a more informative comparison between CCVD and FSP films the maximized response at optimal film thickness should be investigated in the future.[47]

4.4.3. *Mechanical Stability of Physically Bounded Particulate or Highly Porous Films*

A main drawback of FSP-made SnO_2 films is their poor mechanical stability. In fact, while high-temperature deposition, as in CCVD, leads to formation of thick sintering necks and chemical bonding (Figure 15a,b), low-temperature dep-

osition, as in FSP, leads to lace-like structures (Figure 15c,d) held together by relatively weak Van der Waals forces. As a result, as-deposited FSP films are mechanically unstable.[51]

The poor mechanical stability of FSP films is not new and it was the main reason they were discarded from industrial applications in the past. In fact, aerosol deposition of Al_2O_3, Mn_2O_3, ZrO_2, and Y_2O_3-ZrO_2 nanoparticle films was obtained as early as in 1997 by flame spray of organometallic precursors.[137] Nevertheless, it was reported that "*the flame spray synthesis process was found more suitable for producing powders than producing deposits. The deposition efficiencies of the coatings were less than 10 %. Moreover, coating had a powdery structure with almost not adhesion to the substrate*".[137]

Mechanical stabilization of SnO_2 films on sensor substrates was pursued by annealing them at 500 °C for 10 min in a moving belt oven.[50] Nevertheless, with respect to the sintering behavior of SnO_2,[26] the increase in mechanical stability as a result of such low-temperature annealing, is expected to be small. However, high-temperature (> 1000 °C) annealing may also not be applicable as it was reported that highly porous, particulate films tend to disintegrate above a given sintering temperature.[79]

Recently, stabilization of FSP-made SnO_2 films was achieved by rapid (30 s) in situ annealing with a particle-free flame.[51] The SnO_2 crystal size was not altered while the film porosity was reduced drastically, thus increasing the film mechanical stability.[51] As a result, the stability of wafer-level patterned SnO_2 films on micro-machined gas sensors was sufficient to withstand wafer dicing and water-jet cleaning[51] and could be readily integrated in CMOS-compatible processing.[13,138]

5. Materials by Dry Synthesis

Table 2 gives an overview of most common materials used for gas sensors, including oxides of Sn, Ti, W, and Zn that have been synthesized by the dry methods presented in Table 1. It highlights the different materials mainly in terms of crystallinity obtained and the possibility to add dopants during their synthesis. For comprehensive Reviews on the effect of material properties (composition, size, crystallinity, doping) on gas-sensing characteristics please see the cited references.[3,26] Table 2 also includes the deposited film thickness and a list of gases that have been detected using these sensors and can thus guide the choice of dry method for future work to meet certain specifications of the nanostructured film (grain size, thickness) or the gas sensor (analyte detection).

5.1. Crystallinity and Grain Size

Most dry-deposition methods yield amorphous films that require post-annealing to obtain crystalline structures. This post-annealing is important to achieve stable performance during the typical high operation temperature of metal oxide gas sensors (250–600 °C). Note that Table 2 shows the crystallinity of as-prepared films whenever possible, however, the majority of the studies only report structure and performance of annealed layers.

The experimental conditions during annealing have to be optimized as crystallization is typically accompanied by grain growth and film densification, which could reduce the sensitivity (Figure 3, Figure 4). This structural transformation has been summarized in four stages for the thermal treatment of polycrystalline In_2O_3 films: improvement of structural stability (up to 500 °C), coalescence of grains in agglomerates (500–700 °C), local recrystallization (700–1000 °C), and global recrystallization (> 1000 °C).[26] The heat treatment can have profound effects on sensitivity as it affects the inter-grain and inter-agglomerate contacts that, along with the grains and agglomerates, determine the gas response of a polycrystalline film.[26] Additionally, thermal treatments can change the adsorption behavior of oxygen species on the metal oxide surface that in turn will affect the sensitivity (Figure 2).[26]

Post-annealing temperatures of SnO_2 are typically around 400–500 °C,[76,139] however this strongly depends on the preceding synthesis conditions and/or initial film structure,[26] for example, the atmosphere during RF-SPU.[140] The phase evolution of tin oxide has, for example, been investigated by the thermal oxidation of RGTO-made SnO_2 layers.[117] The films were first deposited by DC-SPU on substrates maintained at a temperature above the Sn melting point, then thermal oxidation was performed.[117] Initially, the deposited β-Sn is partially transformed into SnO, as the oxidation proceeds at higher temperatures the SnO/Sn ratio increases until cassiterite SnO_2 is formed at approximately 500 °C.[117]

In situ control of film crystallinity during deposition is typically achieved by heating the target substrates. Although this directly results in crystalline films, the approach can have limitations if applied to heat-sensitive substrates, for example, CMOS micro-sensors.[51] Figure 16 shows X-ray diffraction (XRD) patterns of SnO_2 films deposited by SP on borosilicate glass substrates kept at 300–500 °C.[141] Films deposited at 300 °C were predominantly amorphous and became crystalline (cassiterite tetragonal structure) as the substrate temperature increased.[141] This change is accompanied by SnO_2 crystallite growth from 12 to 48 nm between 350 and 500 °C, respectively, this is also evident from an increase in the intensity of the XRD peaks.[141] A similar evolution of crystallinity and crystallite size has been reported for SnO_2 films deposited by PLD on substrates maintained at room temperature and up to 400 °C.[123]

Similarly, as-deposited amorphous TiO_2 films typically need to be heated to 400–500 °C to transform into the anatase phase and to 700–800 °C to give the rutile phase, however even higher temperatures might be required for complete recrystallization to rutile.[161,167] Titania layers of FSP-made nanoparticles but deposited from the wet phase undergo a nearly complete phase transformation from anatase to rutile after 6 h at 900 °C, however the crystallites grow from 20 nm in the anatase phase to 160 nm in the rutile phase.[202] This growth results in a loss of sensitivity and a change from n- to p-type response,[202] this crossover is expected to occur at compositions between 75 wt % and pure rutile.[203] Again this emphasizes the importance of controlled heat treatments, as they can drastically change the sensing properties of the films.

Table 2: Gas-sensing films of different materials produced by the dry methods presented in Table 1.[a]

Material	Synthesis method	Crystal phase	Grain size* [nm]	Film thickness [nm]	Dopant	Analyte	References
Cr	PLD	$CrTiO_3$	–	120–200	Ti		[142]
Fe	ALD	α-Fe_2O_3	–	100		CO	[143]
	PECVD	α-Fe_2O_3	17	100–300		CO, EtOH	[144, 145]
	RF-SPU	α-Fe_2O_3	–	–		C_7H_{16}, C_5H_{12}, C_8H_{18}, EtOH, H_2, Tol	[146]
In	PLD	In_2O_3	–	500	In(acac)	NO_x, O_3	[147]
	RF-SPU	In_2O_3	–	300–500	MgO, ZnO	Cl_2	[148]
Sn	ACVD	SnO_2	6–15	200	Pd	CH_4, CO, EtOH, H_2	[97, 98, 104, 105, 149]
	ALD	SnO_x, SnO_2	–	1.5–110		CO	[72, 76]
	CCVD	SnO_2	30	1000		EtOH	[74]
	DC-SPU	SnO_2	–	1500–2000	Pd	LPG	[4]
	EVP	SnO_2	5–20	10000		EtOH	[21]
	FSP	SnO_2	5–25	1000–40000	Pt, SiO_2	CO, EtOH	[13, 32, 50, 51, 138]
	HWLP	SnO_x	20	1500	Ag	EtOH	[39]
	IAD	am, SnO_x, SnO_2	8–30	100–500	Ca, Pt	CH_4, C_3H_8, C_4H_{10}, H_2	[109, 120, 150]
	OMCVD	am, SnO_x, SnO_2	5–30	20–300		CH_4, CO, EtOH, H_2O, H_2S, NO_2	[87, 95, 96]
	MBE	SnO_2	–	30–1000		EtOH	[73, 151]
	PECVD	SnO_x, SnO_2	15–30	70–900	Cu, PdO, Pt, Sb	CH_4, CO, EtOH, Gaso, H_2, H_2S, Tol	[94, 100, 144, 152]
	PLD	SnO_x, SnO_2	4–30	24–6000	Pd, Pt	CO, EtOH, H_2	[75, 89, 112, 123, 153]
	RGTO	SnO_x, SnO_2	5–1500	40–300	Au, Cd, Pt, Ti	Act, CH_4, C_4H_{10}, C_6H_6, CO, EtOH, H_2, NO_2, NO_x	[28, 47, 85, 118, 122, 142, 154]
	RF-SPU	SnO_x, SnO_2	3–150	50–5000	Cu, TiO_2	CO, EtOH, H_2, NO_2	[58, 114, 115, 139, 140, 155, 156]
	SP	SnO_x, SnO_2	8–70	20–250	La	EtOH, H_2	[98, 107, 157, 158]
Ti	ALD	TiO_2		5	Pd	H_2	[159]
	EVP	am, TiO_x, TiO_2	3	100		H_2, NH_3	[160, 161]
	IAD	TiO_2	10–20	300	NiO_x	Act, CO, EtOH, NH_3, NO_2	[162]
	RF-SPU	am, TiO_x, TiO_2	20–100	90–1000	Au, Cr, Fe_2O_3, W, WO_3	CO, EtOH , H_2, NO_2	[163–171]-
	SCBD	am, TiO_2	5–15	50–100		EtOH, MeOH, PrOH	[49, 78, 172, 173]
V	DC-SPU	V_2O_5	–	200		NO	[174]
W	DC-SPU	WO_3 (mo)	–	300		H_2, NO_x, NO_2	[90, 174, 175]
	EVP	am, WO_3	17–800	150–20000		NO, NO_2, NH_3	[176, 177]
	PECVD	am, WO_3	–	100		NO_2	[152]
	PLD	WO_3	–	120–500		NO_x, O_3	[142, 147]
	RF-SPU	am, WO_3	10–400	15–4400	Au, ITO , Pd, Pt, Ru, SnO_2, ZnO	Ben, CH_4, C_2H_4, CO, EtOH, H_2, H_2S, NH_3, NO, NO_2, O_3, SO_2	[123, 178–192]
Zn	EVP	am	–	–	Al	H_2	[160]
	OMCVD	ZnO	20	140	TiO_2	Act, CO, EtOH	[193]
	PLD	ZnO	–	5–400	Al	EtOH	[194]
	RF-SPU	ZnO	50–70	45–390	Al, Al_2O_3, TiO_2, V_2O_5	CO, EtOH, $N(CH_3)_3$	[195–197]
	SP	ZnO	12–400	50–500	Al, CdO, La	Act, C_4H_{10}, CO, EtOH, MeOH, NO_2	[157, 198–201]

[a] Synthesis method: for abbreviations please see Table 1. If grain sizes were not reported, crystallite sizes are listed. Crystal phase: am: amorphous, SnO_x refers to non-stoichiometric phases, such as SnO, Sn_3O_4, SnO_{2-x}. Dopant: In(acac): In-acetylacetonate, ITO: indium tin oxide. Analyte: Act: acetone, Ben: benzene, EtOH: ethanol, Gaso: gasoline, LPG: liquefied petroleum gas, MeOH: methanol, PrOH: propanol, Tol: toluene.

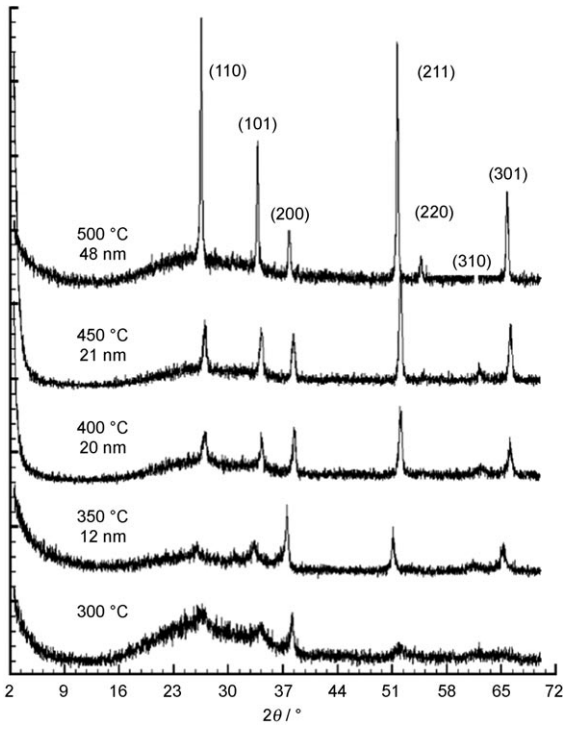

Figure 16. XRD spectra of SnO_2 films deposited by SP on substrates maintained at 300–500 °C. Films deposited at ≥350 °C are polycrystalline and of cassiterite tetragonal structure. The peak intensities, especially those of (110) and (211), increase with increasing temperature as the crystallites grow (12–48 nm).[141]

Phase transformations of tungsten oxides are even more complex as they go through a series of phases from monoclinic ε, triclinic δ, monoclinic γ, orthorhombic β, and tetragonal α-WO_3.[187,204] Annealing temperatures for tungsten oxides are typically in the range of 350–600 °C.[179,184,188,205,206]

For heterogeneous nucleation processes (Figure 7), crystalline films are rarely obtained directly during deposition, unless the substrates are heated as described for PLD and SP.[123,141] However, in processes where the particle- and film-formation zones are decoupled in the reactor (gas-phase nucleation: Figure 7), crystalline films can form directly and post-synthesis annealing is not required. For example, in HWLP, tin oxide particles are formed in an evaporation furnace and further sintered and crystallized in a second furnace at 650 °C prior to deposition on substrates.[39] The deposited $SnO_{1.8}$ nanoparticles are 20 nm in size and can be doped with Ag. Deposition of titania clusters by SCBD can also produce crystalline films in situ without any recrystallization processes after film growth.[207] Brookite and anatase TiO_2 along with substoichiometric (rutile) crystal phases have been detected in as-deposited SCBD films,[49,207] however formation of amorphous layers has also been reported.[78] Crystalline particles are also synthesized by FSP as high temperatures are prevailing during particle formation in the flame.[50] Thus, cassiterite SnO_2,[45] anatase TiO_2,[202] or ε- and γ-WO_3[9] are obtained by flame synthesis and are directly deposited to form particulate films (Figure 4) on substrates (Figure 15). An example of SnO_2 crystallites 16 nm in size made by FSP is shown in Figure 18 a.[32] Often flame-made particles are captured in their metastable phases because of the rapid cooling of the aerosol, as seen for example, for the synthesis of anatase TiO_2 rather than the thermodynamically favorable rutile phase.[202] Further enhancing the cooling of the aerosol by flame quenching also gives access to substoichiometric phases, such as TiO_{2-x}, which exhibit high conductivity.[80]

Highly oriented crystalline films can be obtained by growth on specific substrates, for example, improving the sensitivity[73] or selectivity[208] towards specific gases. For example, the orientation of TiO_2 films can be controlled by RF-SPU growth on sapphire substrates with various orientations.[208] Nearly monocrystalline films are formed by MBE,[151] for example, heteroepitaxial SnO_2 grains oriented along the $<101>$ direction.[73] The lattice parameters of thin-film crystals may not be expected to match those of bulk materials because of the substrate influence, as pointed out for WO_3 films formed by RF-SPU on sapphire.[187] Thus, varying the growth conditions in RF-SPU, random polycrystalline films appeared in either monoclinic or orthorhombic phases as expected for bulk WO_3. In contrast, locally epitaxial films exhibited a cubic phase with many lattice defects (Figure 17).[187]

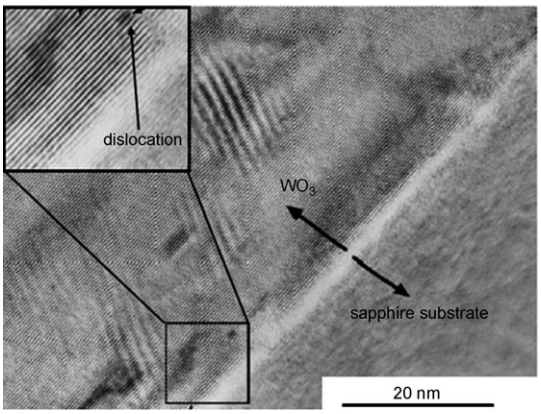

Figure 17. TEM image of a 600 nm thick, locally epitaxial WO_3 film grown by RF-SPU on r-cut sapphire substrate. Edge dislocation defects are visible.[187]

Grain sizes of porous and particulate films (Figure 7) obtained with the described dry methods (Table 1) are typically in the range of a few tens of nanometers, but can vary largely even within the same deposition method (Table 2) as a broad range of process settings are possible (Figure 8). Most importantly, an increase in process or substrate temperature will increase the grain or crystallite size, as seen for the different substrate temperatures[141] in Figure 16. Crystallite sizes of deposited films can be extracted from X-ray diffraction spectra (Figure 16) unless the films are very thin and the signals from the substrate material dominate the spectrum.

However, mostly the grain size will determine the gas-sensing properties and in polycrystalline particles, the crystallite size is smaller than the grain size. The characterization of grain size is challenging in particular for films formed by

heterogeneous nucleation processes (Figure 7). Grain sizes can be directly measured in SEM or AFM images, however at low magnification the sizes can refer to clusters of primary particles or even particle agglomerates as the individual grains are difficult to visualize. In processes that decouple particle formation and film growth (e.g. FSP; Figure 7), particles can be collected separately (not deposited as a film), for example, by filtration from the gas stream. Thus, grain size characterization techniques for nanoparticles, such as nitrogen adsorption and TEM analysis, can be employed more easily, but it has to be assured that these properties are not altered by the film deposition.[51] The effect of grain size polydispersity on gas-sensing properties still has to be addressed. Monodisperse Ag and $SnO_{1.8}$ particles, each 20 nm in size as determined by TEM, have been deposited by HWLP, by size-selecting the synthesized aerosols in differential mobility analyzers.[39]

The grain size will largely govern the gas-sensing properties of nanostructured particulate or porous films; decreasing the grain size increases the sensitivity (Figure 3).[29] However, also the agglomerate sizes and their porosity (or that of the film) will largely influence the sensing characteristics (Figure 4).[26] Table 2 shows the wide variety of film thicknesses that are feasible with most of the aerosol methods, ranging from a few tens of nanometers (thin) to several micrometer (thick) films. However, a fair comparison of film thicknesses is not possible, as information on film porosity is in most cases lacking. Very thin films, such as the ones obtained by ALD, are rather dense (Figure 4), epitaxial, and assumed even to function as a single grain.[72] Thus, highest gas sensitivity is found for film thicknesses comparable to the Debye length of the sensing material.[76] In contrast, deposition of particulate films, for example, by FSP results in high porosity approximately 98% (Figure 15).[50] Thus, although these films are rather thick (Table 2), the effective film thickness is low when taking into account the high porosity of the layer.

5.2. Dopants

Nanoparticles of noble metals (e.g. Pt, Pd, Au, and Ag) and oxides of other elements (e.g. Fe, Zn, Ti) are often used as dopants for gas-sensing metal oxides and they can act as adsorption sites for analytes, surface catalysts, or as elements that improve the thermal stability of the nanostructures.[26] Dopants can be added to sensing films either in situ during film deposition or by a combination of several processes. Typically a good dispersion of the dopant particles over the surface of the base oxide materials is desired (e.g. for noble metals), however mixed oxides (e.g. solid solutions) and segregated structures (e.g. oxide multilayers) have also been investigated. Nobel metals typically act as catalyst on the particle surface and rarely influence the electronic structure of the semiconductor, in contrast to elements such as Fe, Zn, Ti, which may enter the crystal lattice forming a "mixed oxide semiconductor".

In sputtering processes, targets can be prepared from a mixture of elements which allows their simultaneous deposition as has been shown for Cu-doped SnO_2[155] or Al_2O_3-, TiO_2-, or V_2O_5-doped ZnO films by RF-SPU.[196] Dopants can also readily be added in situ during FSP synthesis of nanoparticles.[65] The vapor pressure of noble metals is often higher than that of the supporting metal oxide. Thus the metal oxide particles, such as SnO_2 or TiO_2, form first in the flame and the noble metal clusters nucleate heterogeneously on the support surface. This sequence has been shown for example, for Pt,[50] Au,[209] and Cu,[210] and the doped particles can be directly deposited on sensor substrates.[50] Mixed-metal oxides can also be synthesized by FSP. An example is given in Figure 18b,c for SiO_2-doped SnO_2 particles produced in one step by FSP. The sinter neck size can be controlled by addition of low amounts of silica thus enhancing the sensitivity.[32] The SiO_2-doping gives improved thermal stability of the gas-sensing nanostructures.

Often a combination of techniques is applied to deposit dopant particles, for example, by sputtering of gold nanoparticles onto a SnO_2 film formed by RGTO (Figure 12b).[14] Figure 19a shows an annealed (at 500 °C) TiO_2 film synthesized by ALD on a Si/SiO_2 substrate and subsequent sputtering of Pd, where the Pd nanoparticles act as catalysts for hydrogen sensing at room temperature.[159] Palladium

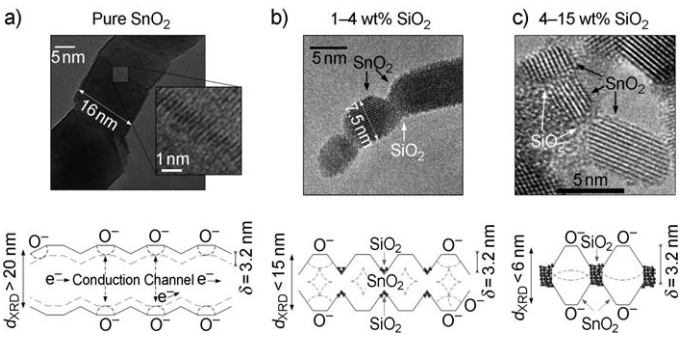

Figure 18. Control of the sintering neck size and shape and thus of the sensing mechanisms of FSP-made SnO_2 nanoparticles by co-synthesis of SiO_2. a) Pure SnO_2 particles form large sinter necks between the crystallites and thereby have only limited sensor response. b) Co-synthesis of SiO_2 decreases and stabilizes the neck size leading to ultrahigh sensitivity. c) Increasing further the SiO_2-content isolates the sensitive SnO_2 and thereby drastically reduces the sensor response. For more details see Ref. [32].

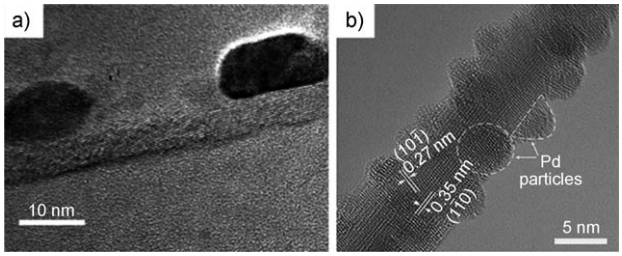

Figure 19. a) Cross-sectional HRTEM image of a compact, polycrystalline TiO_2 film, 5 nm thick, grown by ALD. The lattice planes corresponding to anatase (101) are parallel to the Si/SiO_2 substrate. Well isolated Pd nanoparticles about 20 nm in size are on the underlying TiO_2 film.[159] b) HRTEM image of Pd-doped SnO_2 nanorods.[86] The SnO_2 nanorod film was obtained by PECVD, while the Pd nanoparticles were deposited by electron beam evaporation.

nanoparticles have also been deposited by electron beam evaporation on SnO_2 nanorods formed by PECVD.[86] Figure 19b shows the well-dispersed Pd nanoparticles with an average size of 3 nm that exhibited an improved sensitivity towards H_2 compared to undoped SnO_2 nanorods. Improved sensitivity has also been reported for composite materials where layers of different oxides are applied by several processes in multiple steps. Sandwich structures of SnO_2 and CuO have been developed by wet impregnating a CuO layer on top of a SnO_2 layer formed by PECVD.[152] Double-layer thin films of SnO_2 and Fe_2O_3 have also been manufactured with PECVD and subsequently doped with Pd in the wet phase.[144]

6. Applications of Semiconductor Gas Sensors Prepared by Dry Synthesis

Semiconductor gas sensors have been tested in a plethora of applications including environmental monitoring, workplace safety, process control, and medical diagnostics. Examples of analytes and their targeted detection limits in several applications are given in Table 3. These are correlated with

Table 3: Analytes and approximate detection threshold in various applications.[a]

Application	Analyte	Detection threshold [ppm]	Process	Material	Response [–] to gas [ppm]	LOD [ppm]	Process T [°C]	Operating T [°C]	Ref.
Environmental	NO_2	0.1	ACVD	WO_3	79.6 (0.2)	0.2	350	150	[219]
			CVD	C-Sn	5 (1)	1	500	200	[220]
			CVD	CeO_2	38 (1)	1	400	200	[221]
			EVP	WO_3	7.1 (1)	1	600	200	[222]
			RF-SPU	SnO_2	43 (0.1)	0.05	375	150	[214]
	O_3	0.02	EVP	WO_3	17 (0.08)	0.08	600	400	[222]
			RF-SPU	WO_3	15 (0.03)	0.03	450	523	[179]
			RGTO	Fe:In_2O_3	100 (0.06) at 50% r.h.	0.06	600	400	[223]
			RGTO	SnO_2	10 (0.05)	0.05	600	350	[224]
Process Control and Safety	CH_4	100	EVP	Bi:SnO_2	0.03 (100)	100	600	450	[225]
			RGTO	Ti:SnO_2	0.9 (150)	150	260	400	[118]
	CH_2O	0.01	RF-SPU	NiO	0.105 (0.75)	0.75	450	150	[226]
	CO	10	FSP	Pt:SnO_2	3.4 (10) at 25% r.h.	1	220	450	[51]
			OMCVD	SnO_2	0.53 (10)	1	250	350	[95]
			RF-SPU	Fe:TiO_2	30 (15) at 30% r.h.	15	300	300	[163]
			RF-SPU	MoO_3	1 (10)	1	500	400	[227]
	EtOH	100	ACVD	WO_x	7 (20)	20	625	400	[228]
			CCVD	SnO_2	279 (100)	100	850	300	[74]
			FSP	Si:SnO_2	318 (50)	10	220	320	[32]
			MBE	SnO_2	1.8 (100) at 40% r.h.	100	550	400	[73]
			OMCVD	SnO_2	8 (100)	100	600	500	[87]
			PECVD	Pd:SnO_2	14 (50)	50	600	300	[86]
			PECVD	SnO_2	14 (50)	10	80	450	[94]
			PLD	SnO_2	6 (60)	60	500	450	[75]
			RF-SPU	SnO_2	1.5 (100)	10	400	350	[113]
	H_2	1000	EVP	Bi:SnO_2	20 (1000)	100	200	450	[229]
			IAD	SnO_x	0.99 (1000)	100	500	250	[108]
			MBE	SnO_2	3.5 (1000)	1000	550	400	[73]
			RF-SPU	MoO_3	18 (1000)	1000	500	300	[230]
			RF-SPU	SnO_2	40 (1000)	500	600	550	[116]
	H_2S	10	CVD	Cu:SnO_2	10^6 (10)	5	550	140	[231]
			EVP	Cu:SnO_2	500 (10)	0.02	600	200	[232]
			RF-SPU	Pt:WO_3	300 (10)	1	650	220	[233]
			RGTO	SnO_2	208 (10)	0.1	527	500	[234]
	NH_3	10	EVP	In:ZnO	1.7 (10)	1	500	400	[235]
			RF-SPU	CuBr	78 (10)	1	350	RT	[236]
			RF-SPU	WO_3	1 (10)	10	400	350	[237]
	SO_2	10	DC-SPU	SnO_2	120 (100)	2	520	150	[238]
			OMCVD	SnO_x	14.8 (10)	10	RT	268	[239]
			RF-SPU	Bi:WO_3	1 (10)	1	400	180	[240]
Medical	Act	0.1							
	Ethane	0.01							
	Isoprene	0.01							
	NO	0.01							

[a] Response to reducing gas: $R_{air}/R_{gas}-1$. Response to oxidizing gas: $R_{gas}/R_{air}-1$. Analyte concentrations given in parenthesis. LOD: Limit of detection.

different production processes to make sensing films with different materials, mainly SnO_2, TiO_2, and WO_3. The responses in the range of the detection threshold needed for the specific application are described along with the lowest limit of detection (LOD). Information about the process maximum temperature and operating temperature are listed in Table 3. Dry methods are capable of producing semiconductor films for gas sensors with a wide spectrum of materials exhibiting good long-term stability and high sensitivity towards a range of analytes (Tables 1 and 2). However, only a few of the developed gas-sensing films have been integrated in ready-to-use devices and tested in target applications. The operation of such gas-sensing devices is challenging as the "real" test environment is complex (variations in temperature, relative humidity, interfering gases etc.) and the processing of collected data requires sophisticated electronics and algorithms. Very high sensitivity, rapid response and recovery times (for low molecular weight compounds), portability, and low cost are often regarded as the benefits of devices operating with metal oxide semiconducting gas sensors.[211] However, disadvantages include the required high operation temperature, high power consumption, sulfur and weak acid poisoning, and sensitivity to humidity.[211] A major drawback is also the lack of selectivity in the presence of interfering gases. This problem has been resolved partly by careful materials' engineering (e.g. control of crystal phases, addition of dopants), use of filters in the devices (e.g. to control the relative humidity) and the arrangement of several sensors in arrays (e.g. electronic noses). In the following Sections, examples of gas sensors applied in environmental monitoring, process control, and medical diagnostics will be given.

6.1. Environmental Monitoring

Gas sensing is important for a number of environmental applications,[212] both outdoor and indoor. Polluting gases typically have to be detected well below the maximum authorized threshold concentration set by federal agencies so as to assure accurate and continuous monitoring of pollution episodes.[213]

6.1.1. Outdoor Air Quality

Urban pollution has become a serious issue for public health, evoking strict emission regulations and a need for more accurate air-quality monitoring.[213] The most common air pollutants include nitrous oxide (NO_x), fine suspended particulate matter (PM), carbon monoxide (CO), volatile organic compounds (VOCs), and ozone (O_3), with the latter evoking the most widespread and acute environmental concern.[215] Ozone and NO_2 are taken as examples in Table 3. It appears that the detection threshold required for the specific application is barely reached by aerosol methods. However, for example, RF-SPU SnO_2 reached 0.1 ppm NO_2 detection with a relatively high response (43) while RGTO-made SnO_2 was able to detect down to 0.05 ppm O_3. Typically air-pollutant measurements are carried out with rather expensive and time-consuming analytical instruments, such as gas chromatography (GC), chemiluminescence measurement, mass spectrometry (MS), optical and infrared spectroscopy.[215] These instruments are precise, however difficult to apply for real-time monitoring in the field and thus mobile and cheap complimentary devices are sought.

Prototypes of mobile microstations based on SnO_2 sensors can detect O_3 and NO_x concentrations down to 15 and 50 ppb, respectively, and CO concentrations down to 3 ppm in air, which fulfills the requirements for the lower threshold detection limits (Table 3).[216] Operating temperature of these prototypes were rather low (120–140 °C) with fast response times (1 min) and electronics that allow measurements every 10–20 s.[213] The final device could operate at relative humidity and temperature ranging from 10–100 % and 5–60 °C, respectively. A device based on a ZnO sensor has also been developed to receive and transmit (through a wireless geographic information system (GIS) network) data as a rapid air-pollution monitoring tool to the general public.[217] A portable environmental monitoring system with micro-sensor arrays based on pure and Pd-doped SnO_2 thin films (100–140 nm) has been assembled and tested for detection of ethanol and CH_4.[218]

6.1.2. Indoor Air Quality

Indoor air quality monitoring is often facilitated by a more constant environment (e.g. temperature, humidity, interfering gases) compared to outdoor measurements. Formaldehyde is one of the most common indoor air pollutants as formaldehyde resins are often used in construction materials and it is considered a carcinogen. Micro gas sensors with sensitive SnO_2–NiO films have been developed that can detect 0.06 ppm of formaldehyde even in the presence of interference gases, such as alcohol, acetone, toluene, and α-pinene.[241] Sensor data collected with a MEMS (microelectromechanical system) metal oxide array (pure, Pd- and Pt-doped SnO_2) have been combined with human sensory data to assess the effect of cigarette smoke, fast-food odor, manure and bio-effluents, on the air quality in a car cabin for the design of demand-controlled ventilation systems.[242]

6.2. Process Control and Safety

Gas-monitoring systems are essential constituents of process control to ensure product quality. Metal oxide gas sensors have been tested for some applications to replace or complement more bulky and expensive analysis equipment such as gas chromatographs (GC), with most studies focused on monitoring the freshness of food.[243] Storage life of food is often limited by changes in flavor during spoilage. Different volatile aroma compounds are present during each phase of spoilage and characterize the aroma. The changes of aroma (including compounds such as propanone, butanol, and trimethylamine as determined by GC) during deterioration of fish has been measured with SnO_2 sensors.[243]

Metal oxide semiconductors are often found in electronic-noses (systems that include an array of sensing elements

coupled with suitable statistical methods). This set up enables the distinction of different gases by the pattern of response of individual sensors and thus the recognition of complex odors.[244,245] Electronic noses have been applied to several food matrices, such as milk,[116] tomatoes,[246] olive oils[247,248] and meat.[249] Sensor arrays, including films of copper, zinc, and tin oxide, coupled with a neural network can classify fish species and day of degradation with a resolution of a single day.[250] The applicability of SCBD-made TiO_2 thin films in electronic-nose gas-sensor arrays has been demonstrated and tested in discrimination and recognition of volatile organic compounds (VOCs).[251]

Solid-state gas sensors are mostly needed for safety control as toxic and explosive gases have caused many accidents. CO is one of the most important examples, and the detection of CO by a simple device is an important area of research.[252] Some methods used to produce detectors sensitive to low concentrations of CO are listed in Table 3. Safety on the roads can be improved by new simple and precise ethanol sensors that can be incorporated in alcohol breath analyzers. In fact, many methods are suitable for producing ethanol sensors, mainly based on SnO_2. Furthermore, gases such as H_2 are highly explosive and the monitoring of eventual leakage is important. Exhaust gases from metallurgical industries, such as SO_2, are acutely toxic and cause problems such acid rain, photochemical smog, and corrosion. Sensor materials prepared by different dry methods, such as sputtering or CVD (Table 3) fulfill the required detection threshold for the process application to monitor industrial emissions.

6.3. Medical Diagnostics

Breath analysis is a non-invasive, painless diagnostic method that has the potential to complement classical methods such as biopsy, blood and urine sampling.[253–257] The Ancient Greeks had already recognized that the sweet smell of acetone in breath accompanies uncontrolled diabetes, a fishy smell is a result of liver disease, and a urine-like smell is related to kidney failure. Modern breath analysis developed in the 1970s when Linus Pauling detected around 200 different VOCs in exhaled air by GC. The main components of breath are N_2, O_2, CO_2, H_2O, and inert gases. The remaining small fraction consists of more than 1000 trace volatile organic compounds (VOCs) with concentrations in the range of parts per million (ppm) to parts per trillion (ppt) by volume.[256,258,259] Compounds with relatively high concentrations in exhaled breath include ammonia (median concentration: 833 ppb), acetone (477 ppb), isoprene (106 ppb), methanol (461 ppb), ethanol (112 ppb), propanol (18 ppb) and acetaldehyde (22 ppb).[254] Analysis of human breath samples by various analytical methods has shown a correlation between the concentration patterns of VOCs and the occurrence of certain diseases. For example, ethane and pentane concentrations in breath were elevated in inflammatory diseases.[260,261] Acetone was linked to dextrose metabolism and lipolysis[262] and isoprene to cholesterol biosynthesis. Liver failure and allograft rejection result in elevated concentration of exhaled sulphur-containing compounds.[263] Atopic asthma and lung inflammation increase the concentration of exhaled NO/NO_2.[264,265] Looking at a set of volatile markers may even enable recognition and diagnosis of complex diseases, such as lung and breast cancer.[266]

Techniques for breath analysis have progressed considerably the recent years,[267] however the devices have to fulfill the requirements of high sensitivity, high selectivity, and fast response to the analyte; low cross sensitivity to humidity; small size and simplicity; and low production and maintenance costs. Owing to technical problems of sampling or analysis and a lack of standardization, huge variations exist between results of different studies[266] and thus breath analysis has not yet been introduced to clinical practice.[268] One possibility is the use of sensor arrays (electronic noses) that bear the advantage of low fabrication cost and near-patient diagnostics compared to MS-based analytical instrumentation.[269] Such arrays can contain up to 40 sensor elements based on RF-sputtered WO_3 and SnO_2 films for the sensitive detection of several breath components with small cross sensitivity to ethanol or humidity.[270] Sensor arrays of SnO_2 have been optimized to detect acetone and tested to discriminate diabetic from non-diabetic volunteers.[137] Nanosized γ-Fe_2O_3 sensors can also selectively detect 1 ppm of acetone in the background of human breath.[271] Epitaxially oriented polycrystalline WO_3-based thin films made by RF magnetron sputtering are highly sensitive to nitrogen dioxide.[272] Monitoring of NO (0–100 ppb) in human breath with such sensors is achieved by oxidation of NO with an oxidizing agent and removal of interfering compounds (such as isoprene) by a non-polar molecular sieve filter.[272] Although chemoresistive gas sensors synthesized by aerosol routes are sensitive to many gases and VOCs, to date they do not reach the required low-concentration sensitivities for an application such as breath analysis for medical diagnostics (Table 3). Nevertheless, such detectors have already been produced for some analytes by wet methods. For example, low concentrations of acetone (0.2 ppm) have already been selectively detected by flame-made WO_3 deposited by drop-coating onto sensor substrates.[9]

6.4. Alternative Applications of Metal Oxide Films

Films deposited by dry methods can be used in a wide variety of applications apart from gas sensors, as these techniques enable rather fast and cheap processing and precise control of material and structural properties, as has been shown for example, for ALD.[64] Material properties for a specific application can be optimized by growing functional oxides in a particular direction as has been demonstrated by MBE and PLD to synthesize ferroelectrics, ferromagnets, and combinations thereof.[66] Dilute ferromagnetic semiconducting oxides are obtained by doping materials, such as ZnO, TiO_2, and SnO_2 with transition metals by PLD, MBE, and RF-SPU.[273] Transparent ZnO films formed by RF-SPU or PLD are suitable as thin-film transistors for large area, flexible electronics.[274] Films of $LiMn_2O_4$ for electrodes in lithium-ion

batteries have been deposited by FSP and stabilized by in situ annealing.[275]

Photocatalytic films of ZnO, SnO_2, WO_3, and Fe_2O_3 are applied in a range of environmental applications for the degradation of organic pollutants.[276] Films of photoactive TiO_2[277] are commonly used for purification of indoor VOCs and can be deposited by CVD, MOCVD, or DC/RF-SPU.[162] Flame-made TiO_2 films have also been applied in water-splitting photocells achieving a UV-light to hydrogen conversion efficiency of 11 %.[82]

An opportunity is in the field of dye-sensitized solar cells (DSSCs) that could replace conventional solar cells based on photovoltaic devices.[278] The main drawback of DSSCs is their low efficiency, however, this could be improved by novel processing techniques, that facilitate manufacturing and allow the production of flexible, solid-state solar cells.[279] Deposition of a nanometer-thick coating of an insulating oxide over the semiconducting film in these solar cells may reduce recombination losses.[280] Titania films deposited by flame aerosol reactors have already been tested as DSSCs and gave a maximum efficiency of 6.0 %.[81,82]

7. Summary and Outlook

Dry processes allow the rapid and scalable synthesis of metal oxide, nanostructured films for application as semiconductor gas sensors. A great variety of pure and doped, single and mixed oxides are feasible, and allow control over the growth of their crystal phase and planes. Furthermore, dry processes offer a superior control than wet methods over film morphology in terms of thickness and porosity which has important implications for the modulation of the sensor properties. The control of both material characteristics as well as film structural parameters is feasible.

Completely dense films are obtained by controlling the deposition rate to the substrate on the atomic or molecular scale with accurate ALD or MBE methods. The thickness and roughness of these gas-tight films can be optimized to provide sufficient sensitivity in agreement with the theoretically calculated space-charge thickness (Debye length).

Porous films can be deposited by several methods including spray pyrolysis, sputtering, PLD, CCVD, and RGTO. Although they are characterized by an inhomogeneous morphology consisting of particulate and dense regions, their total porosity is controllable by varying standard operation parameters, such as temperature, pressure, and precursor feed rate. A correct choice of these parameters leads to sufficient penetration of the gas into the film, while preserving small grains, and thereby the high sensitivity observed for CCVD-made films. Furthermore, these methods allow tailoring of the crystal-plane orientation during film growth, which could be an important parameter to improve the poor selectivity of metal oxide sensors.

Deposition of airborne nanoparticles from aerosol sources such as HWLP, FSP, and SCBD leads to the synthesis of particulate films, where grain and crystal size, porosity and thickness are freely adjustable parameters. This novel category of deposition methods combines the good control over the grain properties typical of (thick film) wet methods with the precise control over film thickness of (thin film) aerosol processes. The sensor response obtained by these aerosol methods is often higher than that by classical dry methods. Furthermore, film morphologies that are more homogenous than in wet or classical dry methods are obtained. Nevertheless, the role of grain size polydispersity, sinter neck size, and agglomeration on the performance requires further research. The mechanical stability of such particulate films is generally poor but could be increased by appropriate post-synthesis treatment.

In conclusion, a wide spectrum of analytes can be detected already with metal oxide gas sensors made by dry-synthesis methods, however few of the synthesized films have been tested in target applications under "real" measurement conditions (e.g. presence of interference gases, variation in temperature and relative humidity). Future research should address gas-sensor selectivity and the construction of smart devices for the target applications. Incorporation of these sensing films in ready-to-use devices, might pose further requirements on the sensors, such as deposition on heat-sensitive substrates and high selectivity even at the cost of lower sensitivity.

We express our gratitude to Prof. S. E. Pratsinis (Particle Technology Laboratory, Department of Mechanical and Process Engineering, ETH Zurich) for his support and guidance.

Received: July 11, 2009
Revised: October 31, 2009
Published online: August 18, 2010

[1] R. K. Douglas, S. Alexander, *Angew. Chem.* **2008**, *120*, 6652; *Angew. Chem. Int. Ed.* **2008**, *47*, 6550.
[2] A. R. Baker, J. G. Firth, *Min. Eng.* **1969**, 237.
[3] G. Eranna, B. C. Joshi, D. P. Runthala, R. P. Gupta, *Crit. Rev. Solid State Mater. Sci.* **2004**, *29*, 111.
[4] S. Majumder, S. Hussain, R. Bhar, A. K. Pal, *Vacuum* **2007**, *81*, 985.
[5] P. Massok, M. Loesch, D. Bertrand, *Sens. Actuators B* **1995**, *25*, 525.
[6] A. Katsuki, K. Fukui, *Sens. Actuators B* **1998**, *52*, 30.
[7] J. S. G. Dos Santos-Alves, R. F. Patier, *Sens. Actuators B* **1999**, *59*, 69.
[8] J. J. Ho, Y. K. Fang, K. H. Wu, W. T. Hsieh, C. H. Chen, G. S. Chen, M. S. Ju, J. J. Lin, S. B. Hwang, *Sens. Actuators B* **1998**, *50*, 227.
[9] L. Wang, A. Teleki, S. E. Pratsinis, P. I. Gouma, *Chem. Mater.* **2008**, *20*, 4794.
[10] T. Seiyama, A. Kato, K. Fujiishi, M. Nagatani, *Anal. Chem.* **1962**, *34*, 1502.
[11] N. Taguchi, US Patent 3695848, **1972**.
[12] N. S. Baik, G. Sakai, N. Miura, N. Yamazoe, *Sens. Actuators B* **2000**, *63*, 74.
[13] S. Kühne, M. Graf, A. Tricoli, F. Mayer, S. E. Pratsinis, A. Hierlemann, *J. Micromech. Microeng.* **2008**, *18*, 035040.
[14] I. Elmi, S. Zampolli, E. Cozzani, F. Mancarella, G. C. Cardinali, *Sens. Actuators B* **2008**, *135*, 342.
[15] R. S. Juvet, S. Dalnogare, *Anal. Chem.* **1964**, *36*, 36R.
[16] T. Seiyama, S. Kagawa, *Anal. Chem.* **1966**, *38*, 1069.

[17] M. Nitta, S. Kanefusa, M. Haradome, *J. Electrochem. Soc.* **1978**, *125*, 1676.
[18] M. Graf, A. Gurlo, N. Barsan, U. Weimar, A. Hierlemann, *J. Nanopart. Res.* **2006**, *8*, 823.
[19] M. Graf, D. Barrettino, S. Taschini, C. Hagleitner, A. Hierlemann, H. Baltes, *Anal. Chem.* **2004**, *76*, 4437.
[20] U. Frey, M. Graf, S. Taschini, K. U. Kirstein, A. Hierlemann, *IEEE J. Solid-State Circuits* **2007**, *42*, 441.
[21] H. Ogawa, M. Nishikawa, A. Abe, *J. Appl. Phys.* **1982**, *53*, 4448.
[22] P. G. Harrison, M. J. Willett, *J. Chem. Soc. Faraday Trans. 1* **1989**, *85*, 1921.
[23] J. Watson, K. Ihokura, G. S. V. Coles, *Meas. Sci. Technol.* **1993**, *4*, 711.
[24] N. Barsan, U. Weimar, *J. Electroceram.* **2001**, *7*, 143.
[25] N. Barsan, U. Weimar, *J. Phys. Condens. Matter* **2003**, *15*, R813.
[26] G. Korotcenkov, *Sens. Actuators B* **2005**, *107*, 209.
[27] A. Gurlo, *ChemPhysChem* **2006**, *7*, 2041.
[28] G. Sberveglieri, G. Faglia, S. Groppelli, P. Nelli in *Proc. 6th Int. Conf. Solid-State Sens. Actuators (Transducers'91)*, San Francisco (USA), **1991**, p. 165.
[29] C. Xu, J. Tamaki, N. Miura, N. Yamazoe, *Sens. Actuators B* **1991**, *3*, 147.
[30] N. L. Wu, S. Y. Wang, I. A. Rusakova, *Science* **1999**, *285*, 1375.
[31] R. W. J. Scott, S. M. Yang, G. Chabanis, N. Coombs, D. E. Williams, G. A. Ozin, *Adv. Mater.* **2001**, *13*, 1468.
[32] A. Tricoli, M. Graf, S. E. Pratsinis, *Adv. Funct. Mater.* **2008**, *18*, 1969.
[33] M. Schweizer-Berberich, J. G. Zheng, U. Weimar, W. Göpel, N. Barsan, E. Pentia, A. Tomescu, *Sens. Actuators B* **1996**, *31*, 71.
[34] C. Bittencourt, E. Llobet, P. Ivanov, X. Correig, X. Vilanova, J. Brezmes, J. Hubalek, K. Malysz, J. J. Pireaux, J. Calderer, *Sens. Actuators B* **2004**, *97*, 67.
[35] L. Mädler, T. Sahm, A. Gurlo, J.-D. Grunwald, N. Barsan, U. Weimar, S. E. Pratsinis, *J. Nanopart. Res.* **2006**, *8*, 783.
[36] G. Korotcenkov, V. Brinzari, Y. Boris, M. Ivanov, J. Schwank, J. Morante, *Thin Solid Films* **2003**, *436*, 119.
[37] S. Harbeck, A. Szatvanyi, N. Barsan, U. Weimar, V. Hoffmann, *Thin Solid Films* **2003**, *436*, 76.
[38] J. Zhang, B. K. Miremadi, K. Colbow, *J. Mater. Sci. Lett.* **1994**, *13*, 1048.
[39] R. K. Joshi, F. E. Kruis, O. Dmitrieva, *J. Nanopart. Res.* **2006**, *8*, 797.
[40] V. A. Chaudhary, I. S. Mulla, K. Vijayamohanan, *Sens. Actuators B* **1999**, *55*, 154.
[41] P. Nelli, G. Faglia, G. Sberveglieri, E. Cereda, G. Gabetta, A. Dieguez, A. Romano-Rodriguez, J. R. Morante, *Thin Solid Films* **2000**, *371*, 249.
[42] L. H. Qian, K. Wang, Y. Li, H. T. Fang, Q. H. Lu, X. L. Ma, *Mater. Chem. Phys.* **2006**, *100*, 82.
[43] C. Xu, J. Tamaki, N. Miura, N. Yamazoe, *J. Mater. Sci.* **1992**, *27*, 963.
[44] P. R. J. Holody, R. E. Soltis, J. Hangas, *Scr. Mater.* **2001**, *44*, 1821.
[45] T. Sahm, L. Mädler, A. Gurlo, N. Barsan, S. E. Pratsinis, U. Weimar, *Sens. Actuators B* **2004**, *98*, 148.
[46] H. Kozuka, S. Takenaka, H. Tokita, T. Hirano, Y. Higashi, T. Hamatani, *J. Sol-Gel Sci. Technol.* **2003**, *26*, 681.
[47] T. Becker, S. Ahlers, C. Bosch von Braunmühl, G. Müller, O. Kiesewetter, *Sens. Actuators B* **2001**, *77*, 55.
[48] A. Rothschild, Y. Komem, *J. Appl. Phys.* **2004**, *95*, 6374.
[49] T. Mazza, E. Barborini, I. N. Kholmanov, P. Piseri, G. Bongiorno, S. Vinati, P. Milani, C. Ducati, D. Cattaneo, A. Li Bassi, C. E. Bottani, A. M. Taurino, P. Siciliano, *Appl. Phys. Lett.* **2005**, *87*, 103.
[50] L. Mädler, A. Roessler, S. E. Pratsinis, T. Sahm, A. Gurlo, N. Barsan, U. Weimar, *Sens. Actuators B* **2006**, *114*, 283.
[51] A. Tricoli, M. Graf, F. Mayer, S. Kühne, A. Hierlemann, S. E. Pratsinis, *Adv. Mater.* **2008**, *20*, 3005.
[52] L. Mädler, H. K. Kammler, R. Mueller, S. E. Pratsinis, *J. Aerosol Sci.* **2002**, *33*, 369.
[53] H. Kim, J. Kim, H. Yang, J. Suh, T. Kim, B. Han, S. Kim, D. S. Kim, P. V. Pikhitsa, M. Choi, *Nat. Nanotechnol.* **2006**, *1*, 117.
[54] S. Kanefusa, M. Nitta, M. Haradome, *IEEE Trans. Electron Devices* **1988**, *35*, 65.
[55] M. E. Franke, T. J. Koplin, U. Simon, *Small* **2006**, *2*, 36.
[56] G. Jimenez-Cadena, J. Riu, F. X. Rius, *Analyst* **2007**, *132*, 1083.
[57] T. Asefa, C. T. Duncan, K. K. Sharma, *Analyst* **2009**, *134*, 1980.
[58] Y. Shen, T. Yamazaki, Z. Liu, C. Jin, T. Kikuta, N. Nakatani, *Thin Solid Films* **2008**, *516*, 5111.
[59] J. H. Lee, *Sens. Actuators B* **2009**, *140*, 319.
[60] A. Gurlo, R. Riedel, *Angew. Chem.* **2007**, *119*, 3900; *Angew. Chem. Int. Ed.* **2007**, *46*, 3826.
[61] T. Michael, *Chem. Eur. J.* **2007**, *13*, 8376.
[62] G. Sberveglieri, *Sens. Actuators B* **1992**, *6*, 239.
[63] A. P. Caricato, A. Luches, R. Rella, *Sensors* **2009**, *9*, 2682.
[64] H. Kim, H. B. R. Lee, W. J. Maeng, *Thin Solid Films* **2009**, *517*, 2563.
[65] R. Strobel, S. E. Pratsinis, *J. Mater. Chem.* **2007**, *17*, 4743.
[66] D. G. Schlom, L. Q. Chen, X. Q. Pan, A. Schmehl, M. A. Zurbuchen, *J. Am. Ceram. Soc.* **2008**, *91*, 2429.
[67] J. N. Zemel, *Thin Solid Films* **1988**, *163*, 189.
[68] S. R. Morrison, *The chemical physics of surfaces*, Plenum, New York, **1977**.
[69] V. N. Mishra, R. P. Agarwal, *Microelectron. J.* **1998**, *29*, 861.
[70] I. Sayago, J. Gutiérrez, L. Arés, J. I. Robla, M. C. Horrillo, J. Rino, J. Getino, J. A. Agapito, *Sens. Actuators B* **1995**, *26*, 19.
[71] A. Rosental, A. Tarre, A. Gerst, T. Uustare, V. Sammelselg, *Sens. Actuators B* **2001**, *77*, 297.
[72] A. Rosental, A. Tarre, A. Gerst, J. Sundqvist, A. Hårsta, A. Aidla, J. Aarik, V. Sammelselg, T. Uustare, *Sens. Actuators B* **2003**, *93*, 552.
[73] M. Kroneld, S. Novikov, S. Saukko, P. Kuivalainen, P. Kostamo, V. Lantto, *Sens. Actuators B* **2006**, *118*, 110.
[74] Y. Liu, E. Koep, M. L. Liu, *Chem. Mater.* **2005**, *17*, 3997.
[75] Y. Zhao, Z. Feng, Y. Liang, *Sens. Actuators B* **1999**, *56*, 224.
[76] X. Du, S. M. George, *Sens. Actuators B* **2008**, *135*, 152.
[77] V. Brinzari, G. Korotcenkov, V. Golovanov, *Thin Solid Films* **2001**, *391*, 167.
[78] E. Barborini, G. Bongiorno, A. Forleo, L. Francioso, P. Milani, I. N. Kholmanov, P. Piseri, P. Siciliano, A. M. Taurino, S. Vinati, *Sens. Actuators B* **2005**, *111–112*, 22.
[79] S. K. Andersen, T. Johannessen, M. Mosleh, S. Wedel, J. Tranto, H. Livbjerg, *J. Nanopart. Res.* **2002**, *4*, 405.
[80] A. Teleki, S. E. Pratsinis, *Phys. Chem. Chem. Phys.* **2009**, *11*, 3742.
[81] E. Thimsen, P. Biswas, *AIChE J.* **2007**, *53*, 1727.
[82] E. Thimsen, N. Rastgar, P. Biswas, *J. Phys. Chem. C* **2008**, *112*, 4134.
[83] E. D. Tolmachoff, A. D. Abid, D. J. Phares, C. S. Campbell, H. Wang, *Proc. Combust. Inst.* **2009**, *32*, 1839.
[84] M. Graf, D. Barrettino, K. U. Kirstein, A. Hierlemann, *Sens. Actuators B* **2006**, *117*, 346.
[85] J. G. Partridge, M. R. Field, J. L. Peng, A. Z. Sadek, K. Kalantar-zadeh, J. D. Plessis, D. G. McCulloch, *Nanotechnology* **2008**, *19*, 125504.
[86] Y. C. Lee, H. Huang, O. K. Tan, M. S. Tse, *Sens. Actuators B* **2008**, *132*, 239.
[87] L. Bruno, C. Pijolat, R. Lalauze, *Sens. Actuators B* **1994**, *18*, 195.
[88] G. Korotcenkov, V. Brinzari, J. Schwank, A. Cerneavschi, *Mater. Sci. Eng. C* **2002**, *19*, 73.
[89] R. Dolbec, M. A. El Khakani, A. M. Serventi, R. G. Saint-Jacques, *Sens. Actuators B* **2003**, *93*, 566.

[90] T. S. Kim, Y. B. Kim, K. S. Yoo, G. S. Sung, H. J. Jung, *Sens. Actuators B* **2000**, *62*, 102.
[91] A. Ghicov, P. Schmuki, *Chem. Commun.* **2009**, 2791.
[92] D. Lincot, *Thin Solid Films* **2005**, *487*, 40.
[93] S. Peulon, D. Lincot, *Adv. Mater.* **1996**, *8*, 166.
[94] F. Hellegouarc'h, F. Arefi-Khonsari, R. Planade, J. Amouroux, *Sens. Actuators B* **2001**, *73*, 27.
[95] J. R. Brown, M. T. Cheney, P. W. Haycock, D. J. Houlton, A. C. Jones, E. W. Williams, *J. Electrochem. Soc.* **1997**, *144*, 295.
[96] J. R. Brown, P. W. Haycock, L. M. Smith, A. C. Jones, E. W. Williams, *Sens. Actuators B* **2000**, *63*, 109.
[97] C. G. Borman, R. G. Gordon, *J. Electrochem. Soc.* **1989**, *136*, 3820.
[98] S. Ansari, S. Gosavi, S. Gangal, R. Karekar, R. Aiyer, *J. Mater. Sci. Mater. Electron.* **1997**, *8*, 23.
[99] G. A. Shaw, I. P. Parkin, D. E. Williams, *J. Mater. Chem.* **2003**, *13*, 2957.
[100] P. Y. Liu, J. F. Chen, W. D. Sun, *Vacuum* **2004**, *76*, 7.
[101] S. G. Ansari, Z. A. Ansari, H. K. Seo, G. S. Kim, Y. S. Kim, G. Khang, H. S. Shin, *Sens. Actuators B* **2008**, *132*, 265.
[102] H. Huang, O. K. Tan, Y. C. Lee, M. S. Tse, *J. Cryst. Growth* **2006**, *288*, 70.
[103] G. Korotcenkov, V. Brinzari, J. Schwank, M. DiBattista, A. Vasiliev, *Sens. Actuators B* **2001**, *77*, 244.
[104] D. Briand, M. Labeau, J. F. Currie, G. Delabouglise, *Sens. Actuators B* **1998**, *48*, 395.
[105] A. Salehi, *Sens. Actuators B* **2003**, *96*, 88.
[106] G. Choi, L. Satyanarayana, J. Park, *Appl. Surf. Sci.* **2006**, *252*, 7878.
[107] T. Brousse, D. M. Schleich, *Sens. Actuators B* **1996**, *31*, 77.
[108] W. K. Choi, S. K. Song, J. S. Cho, Y. S. Yoon, D. Choi, H. J. Jung, S. K. Koh, *Sens. Actuators B* **1997**, *40*, 21.
[109] S.-K. Song, J.-S. Cho, W.-K. Choi, H.-J. Jung, D. Choi, J.-Y. Lee, H.-K. Baik, S.-K. Koh, *Sens. Actuators B* **1998**, *46*, 42.
[110] Y.-S. Choe, *Sens. Actuators B* **2001**, *77*, 200.
[111] A. Wisitsoraat, A. Tuantranont, V. Patthanasettakul, T. Lomas, P. Chindaudom, *Sci. Technol. Adv. Mater.* **2005**, *6*, 261.
[112] C. K. Kim, S. M. Choi, I. H. Noh, J. H. Lee, C. Hong, H. B. Chae, G. E. Jang, H. D. Park, *Sens. Actuators B* **2001**, *77*, 463.
[113] C. Bittencourt, E. Llobet, M. A. P. Silva, R. Landers, L. Nieto, K. O. Vicaro, J. E. Sueiras, J. Calderer, X. Correig, *Sens. Actuators B* **2003**, *92*, 67.
[114] G. Micocci, A. Serra, P. Siciliano, A. Tepore, Z. Ali-Adib, *Vacuum* **1996**, *47*, 1175.
[115] M. Di Giulio, G. Micocci, R. Rella, P. Siciliano, A. Tepore, *Sens. Actuators B* **1995**, *23*, 193.
[116] Y.-H. Choi, S.-H. Hong, *Sens. Actuators B* **2007**, *125*, 504.
[117] A. Diéguez, A. Romano-Rodríguez, J. R. Morante, L. Sangaletti, L. E. Depero, E. Comini, G. Faglia, G. Sberveglieri, *Sens. Actuators B* **2000**, *66*, 40.
[118] M. Radecka, J. Przewoznik, K. Zakrzewska, *Thin Solid Films* **2001**, *391*, 247.
[119] Z. N. Tang, G. P. Jiang, P. C. H. Chan, J. K. O. Sin, S. S. Lau, *Sens. Actuators B* **1997**, *43*, 161.
[120] B.-K. Min, S.-D. Choi, *Sens. Actuators B* **2004**, *98*, 239.
[121] H. E. Endres, W. Göttler, R. Hartinger, S. Drost, W. Hellmich, G. Müller, C. Bosch von Braunmühl, A. Krenkow, C. Perego, G. Sberveglieri, *Sens. Actuators B* **1996**, *36*, 353.
[122] J. Szuber, J. Uljanow, T. Karczewska-Buczek, W. Jakubik, K. Waczynski, M. Kwoka, S. Konczak, *Thin Solid Films* **2005**, *490*, 54.
[123] R. Khandelwal, A. P. Singh, A. Kapoor, S. Grigorescu, P. Miglietta, N. E. Stankova, A. Perrone, *Opt. Laser Technol.* **2009**, *41*, 89.
[124] M. K. Akhtar, S. E. Pratsinis, S. V. R. Mastrangelo, *J. Am. Ceram. Soc.* **1992**, *75*, 3408.
[125] S. Vemury, S. E. Pratsinis, *J. Am. Ceram. Soc.* **1995**, *78*, 2984.
[126] S. Vemury, S. E. Pratsinis, L. Kibbey, *J. Mater. Res.* **1997**, *12*, 1031.
[127] K. K. Akurati, A. Vital, R. Hany, B. Bommer, T. Graule, M. Winterer, *Int. J. Photoenergy* **2005**, *7*, 153.
[128] A. Teleki, S. E. Pratsinis, K. Wegner, R. Jossen, F. Krumeich, *J. Mater. Res.* **2005**, *20*, 1336.
[129] S. E. Pratsinis, *Prog. Energy Combust. Sci.* **1998**, *24*, 197.
[130] A. Teleki, R. Wengeler, L. Wengeler, H. Nirschl, S. E. Pratsinis, *Powder Technol.* **2008**, *181*, 292.
[131] M. J. Height, L. Madler, S. E. Pratsinis, F. Krumeich, *Chem. Mater.* **2006**, *18*, 572.
[132] E. Barborini, I. N. Kholmanov, P. Piseri, C. Ducati, C. E. Bottani, P. Milani, *Appl. Phys. Lett.* **2002**, *81*, 3052.
[133] L. Mädler, A. A. Lall, S. K. Friedlander, *Nanotechnology* **2006**, *17*, 4783.
[134] T. D. Elmøe, A. Tricoli, J.-D. Grunwaldt, S. E. Pratsinis, *J. Aerosol Sci.* **2009**, *40*, 965.
[135] A. Tricoli, S. E. Pratsinis, *Int. J. Nanomanufact.* **2010**, in press.
[136] T. Sahm, W. H. Rong, N. Barsan, L. Mädler, S. K. Friedlander, U. Weimar, *J. Mater. Res.* **2007**, *22*, 850.
[137] J. Karthikeyan, C. C. Berndt, J. Tikkanen, J. Y. Wang, A. H. King, H. Herman, *Nanostruct. Mater.* **1997**, *9*, 137.
[138] S. Kühne, M. Graf, A. Tricoli, H. Meier, F. Mayer, S. E. Pratsinis, A. Hierlemann in *Eurosensors X*, *Vol. 2*, Göteborg, Sweden, **2006**, p. 274.
[139] S. I. Rembeza, E. S. Rembeza, T. V. Svistova, O. I. Borsiakova, *Phys. Status Solidi A* **2000**, *179*, 147.
[140] P. Serrini, V. Briois, M. C. Horrillo, A. Traverse, L. Manes, *Thin Solid Films* **1997**, *304*, 113.
[141] T. Serin, N. Serin, S. Karadeniz, H. Sari, N. Tugluoglu, O. Pakma, *J. Non-Cryst. Solids* **2006**, *352*, 209.
[142] S. Nicoletti, S. Zampolli, I. Elmi, L. Dori, M. Severi, *IEEE Sens. J.* **2003**, *3*, 454.
[143] M. Aronniemi, J. Saino, J. Lahtinen, *Thin Solid Films* **2008**, *516*, 6110.
[144] M. S. Tong, G. R. Dai, D. S. Gao, *Vacuum* **2000**, *59*, 877.
[145] B. P. Yan, J. Peng, C. C. Chai, *Thin Solid Films* **1994**, *245*, 225.
[146] K. Siroky, J. Jiresova, L. Hudec, *Thin Solid Films* **1994**, *245*, 211.
[147] R. Frycek, M. Vladimir, V. Martin, V. Filip, M. Jelinek, J. Nahlik, *Sens. Actuators B* **2004**, *98*, 233.
[148] T. Miyata, T. Hikosaka, T. Minami, *Sens. Actuators B* **2000**, *69*, 16.
[149] J. Sundqvist, M. Ottosson, A. Harsta, *Chem. Vap. Deposition* **2004**, *10*, 77.
[150] B.-K. Min, S.-D. Choi, *Sens. Actuators B* **2005**, *108*, 125.
[151] M. E. White, M. Y. Tsai, F. Wu, J. S. Speck, *J. Vac. Sci. Technol. A* **2008**, *26*, 1300.
[152] W. Yuanda, T. Maosong, H. Xiuli, Z. Yushu, D. Guorui, *Sens. Actuators B* **2001**, *79*, 187.
[153] A. Pereira, L. Cultrera, A. Dima, M. Susu, A. Perrone, H. L. Du, A. O. Volkov, R. Cutting, P. K. Datta, *Thin Solid Films* **2006**, *497*, 142.
[154] W. Hellmich, C. Bosch von Braunmühl, G. Müller, G. Sberveglieri, M. Berti, C. Perego, *Thin Solid Films* **1995**, *263*, 231.
[155] V. V. Kissine, S. A. Voroshilov, V. V. Sysoev, *Thin Solid Films* **1999**, *348*, 304.
[156] H. C. Lee, W. S. Hwang, *Appl. Surf. Sci.* **2006**, *253*, 1889.
[157] I. Stambolova, K. Konstantinov, S. Vassilev, P. Peshev, T. Tsacheva, *Mater. Chem. Phys.* **2000**, *63*, 104.
[158] G. Korotcenkov, M. DiBattista, J. Schwank, V. Brinzari, *Mater. Sci. Eng. B* **2000**, *77*, 33.
[159] M. K. Kumar, L. K. Tan, N. N. Gosvami, H. Gao, *J. Phys. Chem. C* **2009**, *113*, 6381.
[160] V. Aroutiounian, V. Arakelyan, V. Galstyan, K. Martirosyan, P. Soukiassian, *IEEE Sens. J.* **2009**, *9*, 9.
[161] D. Manno, G. Micocci, R. Rella, A. Serra, A. Taurino, A. Tepore, *J. Appl. Phys.* **1997**, *82*, 54.

[162] A. Wisitsraat, A. Tuantranont, E. Comini, G. Sberveglieri, W. Modarski, *Thin Solid Films* **2009**, *517*, 2775.
[163] E. Comini, G. Sberveglieri, M. Ferroni, V. Guidi, C. Frigeri, D. Boscarino, *J. Mater. Res.* **2001**, *16*, 1559.
[164] I. A. Al-Homoudi, J. S. Thakur, R. Naik, G. W. Auner, G. Newaz, *Appl. Surf. Sci.* **2007**, *253*, 8607.
[165] I. Alessandri, E. Comini, E. Bontempi, G. Faglia, L. E. Depero, G. Sberveglieri, *Sens. Actuators B* **2007**, *128*, 312.
[166] J. Tan, W. Wlodarski, K. Kalantar-Zadeh, *Thin Solid Films* **2007**, *515*, 8738.
[167] A. Rothschild, F. Edelman, Y. Komem, F. Cosandey, *Sens. Actuators B* **2000**, *67*, 282.
[168] S. J. Kang, C. Kocabas, T. Ozel, M. Shim, N. Pimparkar, M. A. Alam, S. V. Rotkin, J. A. Rogers, *Nat. Nanotechnol.* **2007**, *2*, 230.
[169] M. Ferroni, V. Guidi, G. Martinelli, G. Sberveglieri, *J. Mater. Res.* **1997**, *12*, 793.
[170] M. Ferroni, V. Guidi, G. Martinelli, G. Faglia, P. Nelli, G. Sberveglieri, *Nanostruct. Mater.* **1996**, *7*, 709.
[171] E. Comini, G. Sberveglieri, V. Guidi, *Sens. Actuators B* **2000**, *70*, 108.
[172] A. M. Taurino, S. Capone, P. Siciliano, T. Toccoli, A. Boschetti, L. Guerini, S. Iannotta, *Sens. Actuators B* **2003**, *92*, 292.
[173] A. M. Taurino, S. Capone, P. Siciliano, T. Toccoli, A. Boschetti, L. Guerini, S. Iannotta, *Sens. Actuators B* **2003**, *92*, 292.
[174] S. Capone, R. Rella, P. Siciliano, L. Vasanelli, *Thin Solid Films* **1999**, *350*, 264.
[175] Y. Shen, T. Yamazaki, Z. Liu, D. Meng, T. Kikuta, N. Nakatani, *Thin Solid Films* **2009**, *517*, 2069.
[176] T. Siciliano, A. Tepore, G. Micocci, A. Serra, D. Manno, E. Filippo, *Sens. Actuators B* **2008**, *133*, 321.
[177] H. T. Sun, C. Cantalini, L. Lozzi, M. Passacantando, S. Santucci, M. Pelino, *Thin Solid Films* **1996**, *287*, 258.
[178] M. Di Giulio, D. Manno, G. Micocci, A. Serra, A. Tepore, *J. Phys. D* **1997**, *30*, 3211.
[179] M. Bendahan, R. Boulmani, J. L. Seguin, K. Aguir, *Sens. Actuators B* **2004**, *100*, 320.
[180] R. Boulmani, M. Bendahan, C. Lambert-Mauriat, M. Gillet, K. Aguir, *Sens. Actuators B* **2007**, *125*, 622.
[181] M. H. Yaacob, M. Breedon, K. Kalantar-Zadeh, W. Wlodarski, *Sens. Actuator B* **2009**, *137*, 115.
[182] S. Vallejos, V. Khatko, J. Calderer, I. Gracia, C. Cane, E. Llobet, X. Correig, *Sens. Actuators B* **2008**, *132*, 209.
[183] A. Stankova, X. Vilanova, E. Llobet, J. Calderer, C. Bittencourt, J. J. Pireaux, X. Coffeig, *Sens. Actuators B* **2005**, *105*, 271.
[184] M. Penza, M. A. Tagliente, L. Mirenghi, C. Gerardi, C. Martucci, G. Cassano, *Sens. Actuators B* **1998**, *50*, 9.
[185] M. Penza, C. Martucci, G. Cassano, *Sens. Actuators B* **1998**, *50*, 52.
[186] D. Manno, A. Serra, M. Di Giulio, G. Micocci, A. Tepore, *Thin Solid Films* **1998**, *324*, 44.
[187] L. J. LeGore, R. J. Lad, S. C. Moulzolf, J. F. Vetelino, B. G. Frederick, E. A. Kenik, *Thin Solid Films* **2002**, *406*, 79.
[188] A. Labidi, C. Lambert-Mauriat, C. Jacolin, M. Bendahan, M. Maaref, K. Aguir, *Sens. Actuators B* **2006**, *119*, 374.
[189] V. Khatko, S. Vallejos, J. Calderer, E. Llobet, X. Vilanova, X. Correig, *Sens. Actuators B* **2007**, *126*, 400.
[190] H. Keskinen, A. Tricoli, M. Marjamäki, J. M. Mäkelä, S. E. Pratsinis, *J. Appl. Phys.* **2009**, *106*, 084316.
[191] C. J. Jin, T. Yamazaki, Y. Shirai, T. Yoshizawa, T. Kikuta, N. Nakatani, H. Takeda, *Thin Solid Films* **2005**, *474*, 255.
[192] M. Gillet, K. Aguir, M. Bendahan, P. Mennini, *Thin Solid Films* **2005**, *484*, 358.
[193] D. Barreca, E. Comini, A. P. Ferrucci, A. Gasparotto, C. Maccato, C. Maragno, G. Sberveglieri, E. Tondello, *Chem. Mater.* **2007**, *19*, 5642.
[194] S. K. Kim, J. Y. Son, *Electrochem. Solid-State Lett.* **2009**, *12*, J17.
[195] J. F. Chang, H. H. Kuo, I. C. Leu, M. H. Hon, *Sens. Actuators B* **2002**, *84*, 258.
[196] T. H. Kwon, S. H. Park, J. Y. Ryu, H. H. Choi, *Sens. Actuators B* **1998**, *46*, 75.
[197] S. M. Chou, L. G. Teoh, W. H. Lai, Y. H. Su, M. H. Hon, *Sensors* **2006**, *6*, 1420.
[198] R. Ferro, J. A. Rodriguez, I. Jimenez, A. Cirera, J. Cerda, J. R. Morante, *IEEE Sens. J.* **2005**, *5*, 48.
[199] M. T. Mohammad, A. A. Hashim, M. H. Al-Maamory, *Mater. Chem. Phys.* **2006**, *99*, 382.
[200] P. P. Sahay, R. K. Nath, *Sens. Actuators B* **2008**, *134*, 654.
[201] P. P. Sahay, *J. Mater. Sci.* **2005**, *40*, 4383.
[202] A. Teleki, S. E. Pratsinis, K. Kalyanasundaram, P. I. Gouma, *Sens. Actuators B* **2006**, *119*, 683.
[203] N. O. Savage, S. Roberson, G. Gillen, M. J. Tarlov, S. Semancik, *Anal. Chem.* **2003**, *75*, 4360.
[204] E. Salje, K. Viswanathan, *Acta Crystallogr. Sect. A* **1975**, *31*, 356.
[205] M. T. Ke, M. T. Lee, C. Y. Lee, L. M. Fu, *Sensors* **2009**, *9*, 2895.
[206] M. Stankova, X. Vilanova, E. Llobet, J. Calderer, M. Vinaixa, I. Gracia, C. Cane, X. Correig, *Thin Solid Films* **2006**, *500*, 302.
[207] T. Toccoli, S. Capone, L. Guerini, M. Anderle, A. Boschetti, E. Iacob, V. Micheli, P. Siciliano, S. Iannotta, *IEEE Sens. J.* **2003**, *3*, 199.
[208] W. T. Moon, K. S. Lee, Y. K. Jun, H. S. Kim, S. H. Hong, *Sens. Actuators B* **2006**, *115*, 123.
[209] L. Mädler, W. J. Stark, S. E. Pratsinis, *J. Mater. Res.* **2003**, *18*, 115.
[210] A. Teleki, N. Bjelobrk, S. E. Pratsinis, *Sens. Actuators B* **2008**, *130*, 449.
[211] A. D. Wilson, M. Baietto, *Sensors* **2009**, *9*, 5099.
[212] J. Riu, A. Maroto, F. X. Rius, *Talanta* **2006**, *69*, 288.
[213] M. I. Baraton, L. Merhari, *J. Nanopart. Res.* **2004**, *6*, 107.
[214] M. C. Horrillo, P. Serrini, J. Santos, L. Manes, *Sens. Actuators B* **1997**, *45*, 193.
[215] M. M. Liang, L. H. Guo, *J. Nanosci. Nanotechnol.* **2009**, *9*, 2283.
[216] M. I. Baraton, L. Merhari, *Mater. Sci. Eng. B* **2004**, *112*, 206.
[217] O. Pummakarnchana, N. Tripathi, J. Dutta, *Sci. Technol. Adv. Mater.* **2005**, *6*, 251.
[218] A. Baschirotto, S. Capone, A. D'Amico, C. Di Natale, V. Ferragina, G. Ferri, L. Francioso, M. Grassi, N. Guerrini, P. Malcovati, E. Martinelli, R. Siciliano, *Sens. Actuators B* **2008**, *130*, 164.
[219] S. Ashraf, C. S. Blackman, R. G. Palgrave, S. C. Naisbitt, I. P. Parkin, *J. Mater. Chem.* **2007**, *17*, 3708.
[220] R. Larciprete, E. Borsella, P. De Padova, P. Perfetti, G. Faglia, G. Sberveglieri, *Thin Solid Films* **1998**, *323*, 291.
[221] D. Barreca, E. Comini, A. Gasparotto, C. Maccato, C. Maragno, G. Sberveglieri, E. Tondello, *J. Nanosci. Nanotechnol.* **2008**, *8*, 1012.
[222] C. Cantalini, W. Wlodarski, Y. Li, M. Passacantando, S. Santucci, E. Comini, G. Faglia, G. Sberveglieri, *Sens. Actuators B* **2000**, *64*, 182.
[223] C. Baratto, M. Ferroni, G. Faglia, G. Sberveglieri, *Sens. Actuators B* **2006**, *118*, 221.
[224] T. Becker, L. Tomasi, C. Bosch von Braunmühl, G. Müller, G. Fagli, E. Comini, *Sens. Actuators A* **1999**, *74*, 229.
[225] G. Sberveglieri, *Sens. Actuators B* **1995**, *23*, 103.
[226] C. Y. Lee, C. M. Chiang, Y. H. Wang, R. H. Ma, *Sens. Actuators B* **2007**, *122*, 503.
[227] M. Ferroni, V. Guidi, G. Martinelli, P. Nelli, M. Sacerdoti, G. Sberveglieri, *Thin Solid Films* **1997**, *307*, 148.
[228] S. Ashraf, C. S. Blackman, S. C. Naisbitt, I. P. Parkin, *Meas. Sci. Technol.* **2008**, *19*, DOI: 10.1088/0957-0233/19/2/025203.
[229] G. Sberveglieri, S. Groppelli, P. Nelli, A. Camanzi, *Sens. Actuators B* **1991**, *3*, 183.
[230] C. Imawan, H. Steffes, F. Solzbacher, E. Obermeier, *Sens. Actuators B* **2001**, *78*, 119.

[231] A. Khanna, R. Kumar, S. S. Bhatti, *Appl. Phys. Lett.* **2003**, *82*, 4388.
[232] J. Tamaki, K. Shimanoe, Y. Yamada, Y. Yamamoto, N. Miura, N. Yamazoe, *Sens. Actuators B* **1998**, *49*, 121.
[233] W. H. Tao, C. H. Tsai, *Sens. Actuators B* **2002**, *81*, 237.
[234] G. Sberveglieri, S. Groppelli, P. Nelli, C. Perego, G. Valdre, A. Camanzi, *Sens. Actuators B* **1993**, *15*, 86.
[235] G. Sberveglieri, S. Groppelli, P. Nelli, A. Tintinelli, G. Giunta, *Sens. Actuators B* **1995**, *25*, 588.
[236] P. Lauque, M. Bendahan, J. L. Seguin, K. A. Ngo, P. Knauth, *Anal. Chim. Acta* **2004**, *515*, 279.
[237] B. T. Marquis, J. F. Vetelino, *Sens. Actuators B* **2001**, *77*, 100.
[238] J. Getino, J. Gutierrez, L. Ares, J. I. Robla, M. C. Horrillo, I. Sayago, J. A. Agapito, *Sens. Actuators B* **1996**, *33*, 128.
[239] J. Lancok, A. Santoni, M. Penza, S. Loreti, I. Menicucci, C. Minarini, M. Jelinek, *Surf. Coat. Technol.* **2005**, *200*, 1057.
[240] M. Penza, G. Cassano, F. Tortorella, *Sens. Actuators B* **2001**, *81*, 115.
[241] T. Delclos, C. Aime, E. Pouget, A. Brizard, I. Huc, M. H. Delville, R. Oda, *Nano Lett.* **2008**, *8*, 1929.
[242] M. Blaschke, T. Tille, P. Robertson, S. Mair, U. Weimar, H. Ulmer, *IEEE Sens. J.* **2006**, *6*, 1298.
[243] R. Ólafsson, E. Martinsdottir, G. Ólafsdottir, P. I. Sigfusson, J. W. Gardner in *Sensors and Sensory Systems for an Electronic Nose* (Eds.: J. W. Gardner, P. N. Bartlett), Kluwer Academic Publishers, Netherlands, **1992**, p. 257.
[244] D. James, S. M. Scott, Z. Ali, W. T. O'Hare, *Microchim. Acta* **2005**, *149*, 1.
[245] E. Schaller, J. O. Bosset, F. Escher, *Food Sci. Technol.* **1998**, *31*, 305.
[246] A. H. Gomez, G. X. Hu, J. Wang, A. G. Pereira, *Comput. Electron. Agric.* **2006**, *54*, 44.
[247] D. L. Garcia-Gonzalez, R. Aparicio, *Eur. Food Res. Technol.* **2002**, *215*, 118.
[248] A. Taurino, S. Capone, C. Distante, M. Epifani, R. Rella, P. Siciliano, *Thin Solid Films* **2002**, *418*, 59.
[249] D. D. H. Boothe, J. W. Arnold, *J. Sci. Food Agric.* **2002**, *82*, 315.
[250] J. Hammond, B. Marquis, R. Michaels, B. Oickle, B. Segee, J. Vetelino, A. Bushway, M. E. Camire, K. Davis-Dentici, *Sens. Actuators B* **2002**, *84*, 113.
[251] T. Toccoli, A. Boschetti, L. Guerini, S. Iannotta, S. Capone, P. Siciliano, A. Taurino, in *Proceedings of IEEE Sensors 2002. First IEEE International Conference on Sensors*, IEEE, **2002**, p. 647.
[252] S. J. Jung, H. Yanagida, *Sens. Actuators B* **1996**, *37*, 55.
[253] T. Ligor, *Crit. Rev. Anal. Chem.* **2009**, *39*, 2.
[254] B. Buszewski, M. Kesy, T. Ligor, A. Amann, *Biomed. Chromatogr.* **2007**, *21*, 553.
[255] A. Manolis, *Clin. Chem.* **1983**, *29*, 5.
[256] R. Mukhopadhyay, *Anal. Chem.* **2004**, *76*, 273 A.
[257] W. Miekisch, J. K. Schubert, G. F. E. Noeldge-Schomburg, *Clin. Chim. Acta* **2004**, *347*, 25.
[258] W. Q. Cao, Y. X. Duan, *Clin. Chem.* **2006**, *52*, 800.
[259] M. Phillips, J. Herrera, S. Krishnan, M. Zain, J. Greenberg, R. N. Cataneo, *J. Chromatogr. B* **1999**, *729*, 75.
[260] C. O. Olopade, M. Zakkar, W. I. Swedler, I. Rubinstein, *Chest* **1997**, *111*, 862.
[261] P. Paredi, S. A. Kharitonov, D. Leak, S. Ward, D. Cramer, P. J. Barnes, *Am. J. Respir. Crit. Care Med.* **2000**, *162*, 369.
[262] M. J. Sulway, J. M. Malins, *Lancet* **1970**, *296*, 736.
[263] S. Chen, L. Zieve, V. Mahadeva, *J. Lab. Clin. Med.* **1970**, *75*, 628.
[264] S. A. Kharitonov, P. J. Barnes, *Biomarkers* **2002**, *7*, 1.
[265] F. Di Francesco, R. Fuoco, M. G. Trivella, A. Ceccarini, *Microchem. J.* **2005**, *79*, 405.
[266] M. Phillips, R. N. Cataneo, A. R. C. Cummin, A. J. Gagliardi, K. Gleeson, J. Greenberg, R. A. Maxfield, W. N. Rom, *Chest* **2003**, *123*, 2115.
[267] W. Q. Cao, Y. X. Duan, *Crit. Rev. Anal. Chem.* **2007**, *37*, 3.
[268] T. H. Risby, S. F. Solga, *Appl. Phys. B* **2006**, *85*, 421.
[269] J. W. Gardner, H. W. Shin, E. L. Hines, *Sens. Actuators B* **2000**, *70*, 19.
[270] S. Ehrmann, J. Jungst, J. Goschnick, D. Everhard, *Sens. Actuators B* **2000**, *65*, 247.
[271] S. Chakraborty, D. Banerjee, I. Ray, A. Sen, *Curr. Sci.* **2008**, *94*, 237.
[272] B. Fruhberger, N. Stirling, F. G. Grillo, S. Ma, D. Ruthven, R. J. Lad, B. G. Frederick, *Sens. Actuators B* **2001**, *76*, 226.
[273] S. J. Pearton, W. H. Heo, M. Ivill, D. P. Norton, T. Steiner, *Semicond. Sci. Technol.* **2004**, *19*, R59.
[274] Y. G. Sun, J. A. Rogers, *Adv. Mater.* **2007**, *19*, 1897.
[275] S. Y. Chew, T. J. Patey, O. Waser, S. H. Ng, R. Büchel, A. Tricoli, F. Krumeich, J. Wang, H. K. Liu, S. E. Pratsinis, P. Novák, *J. Power Sources* **2009**, *189*, 449.
[276] H. J. Zhang, G. H. Chen, D. W. Bahnemann, *J. Mater. Chem.* **2009**, *19*, 5089.
[277] X. Chen, S. S. Mao, *Chem. Rev.* **2007**, *107*, 2891.
[278] B. O'Regan, M. Grätzel, *Nature* **1991**, *353*, 737.
[279] J. N. Hart, Y. B. Cheng, G. P. Simon, L. Spiccia, *J. Nanosci. Nanotechnol.* **2008**, *8*, 2230.
[280] E. Palomares, J. N. Clifford, S. A. Haque, T. Lutz, J. R. Durrant, *J. Am. Chem. Soc.* **2003**, *125*, 475.